Time Dependent Shrinkage of Time-Varying Parameter Regression Models

Zhongfang He*

First Version: March 20, 2021

Abstract

This paper studies the time-varying parameter (TVP) regression model in which the regression coefficients are random walk latent states with time dependent conditional variances. This TVP model is flexible to accommodate a wide variety of time variation patterns but requires effective shrinkage on the state variances to avoid over-fitting. A Bayesian shrinkage prior is proposed based on reparameterization that translates the variance shrinkage problem into a variable shrinkage one in a conditionally linear regression with fixed coefficients. The proposed prior allows strong shrinkage for the state variances while maintaining the flexibility to accommodate local signals. A Bayesian estimation method is developed that employs the ancilarity-sufficiency interweaving strategy to boost sampling efficiency. Simulation study and an empirical application to forecast inflation rate illustrate the benefits of the proposed approach.

Keywords: TVP, Bayesian shrinkage, MCMC, Horseshoe, ASIS
JEL Codes: C01, C11, C22, E37

*Email: hezhongfang2004@yahoo.com. Royal Bank of Canada, 155 Wellington St W, Toronto, ON, Canada, M5V 3H6. The views in this paper are solely the author's responsibility and are not related to the company the author works in.

1 Introduction

The time-varying parameter (TVP) regression model allows the coefficients of a linear regression model to vary over time to capture possible model instability and has been widely applied in econometric studies of time series data (Cogley and Sargent (2005), Primiceri (2005), Dangl and Halling (2012), Belmonte et al. (2014)). Granger (2008) shows theoretically that any non-linear model can be approximated by a TVP model. The commonly used configuration of the TVP model specifies the time varying coefficients as latent states that follow independent random walk processes with constant variances. Bitto and Fruhwirth-Schnatter (2019) is a recent contribution that shrinks the variances of the time varying coefficients and is able to automatically discriminate constant coefficients from time varying ones[1]. However the assumption of homoskedastic latent states is inherently restrictive and permits only two types of time variation patterns for each coefficient: either staying constant all the time or changing continuously. Allowing for infrequent parameter shifts and episodical combinations of constant and time-varying coefficients remains a challenge for the TVP model with homoskedastic latent states.

Recent developments in the literature have begun to allow time varying variances in the latent states of TVP models. By allowing the latent state variance to take different values from approximately zero to very large ones at each time t, both constant parameters, continuous and discrete parameter shifts as well as their episodical combinations could be accommodated in the TVP framework. Hence the practitioners can be relieved of the difficult task to pre-determine if potential parameter shifts are continuous as in the conventional TVP models or are infrequent as in the change point literature (e.g. Chib (1998), Dufays and Rombouts (2020)). To allow for heteroskedastic latent states, one strand of the literature directly applies Bayesian global-local shrinkage priors to the differenced latent states[2]. The variance of each differenced latent state is specified as the product of a

[1]Other recent examples of shrinkage TVP models with homoskedastic latent states include Cadonna et al. (2020), Chan et al. (2020) etc.

[2]Another strand of the literature allows heteroskedastic latent states by applying time-dependent spike-and-slab mixture priors for state variances (e.g. Giordani and Kohn (2008), Chan et al. (2012), Hauzenberger (2021), Rockova and McAlinn (2021)) but faces the computational hurdle due to the combinatorial complexity of sampling the mixture indicators of the spike-and-slab priors.

"global"' shrinkage parameter that remains constant and a "local"' shrinkage parameter that can vary over time. The global shrinkage parameter pushes the variance of the latent state towards zero and hence favors a constant coefficient, while the local shrinkage parameter adapts to local signals at each time t and could result in a large overall variance at time t to accommodate possible local parameter shifts. For example, Kowal et al. (2019) and Huber and Pfarrhofer (2021) contain TVP models where the horseshoe prior (Carvalho et al. (2010)) is applied to each differenced latent state. Kowal et al. (2019) further proposes a dynamic horseshoe prior that allows an autoregressive structure in the local shrinkage parameter of each latent state variance and shows superior performance of the resulting TVP models over alternative dynamic shrinkage priors such as the dynamic normal-gamma one of Kalli and Griffin (2014)[3]. In this paper, I will show that both approaches can be improved by borrowing from the "non-centered" parametrization strategy of Fruhwirth-Schnatter and Wagner (2010) and in a computationally efficient fashion.

Shrinking the state variances towards zero amounts to the "variance selection" problem in the literature (Harvey (1989)). Pioneering work on the variance selection problem in the Bayesian framework includes Fruhwirth-Schnatter (2004), Fruhwirth-Schnatter and Wagner (2010), Nakajima and West (2013) and Kalli and Griffin (2014) etc. An attractive idea from Fruhwirth-Schnatter and Wagner (2010) is that by appropriate reparameterization of the original TVP model, the variance selection problem can be recast as a variable selection problem in a conditionally linear regression with the signed square root of the latent state variance being the constant coefficients. Hence the vast literature on variable selection by shrinkage priors can be borrowed on for efficient model estimation. I build on this insight from Fruhwirth-Schnatter and Wagner (2010) and proposes a new hierarchical prior to model the heteroskedasticity in the latent states of TVP models.

Specifically, rather than directly applying shrinkage priors to the time dependent state variances, I consider reparametrizing the random walk TVP model and apply horseshoe shrinkage priors to the signed square root of the state variances. In a nutshell, the resulting prior on each latent state variance is a gamma distribution in which the scale parameter is the product of a time-invariant global shrinkage parameter and a time-varying local

[3]See Hauzenberger et al. (2020) for similar strategies for versions of TVP models where latent states follow independent Gaussian distributions rather than random walks.

shrinkage parameter. While the local shrinkage parameters follow independent inverted beta distributions as in the horseshoe prior, the global shrinkage parameter is a scale-mixture gamma distribution. I label this new shrinkage prior as a *gamma horseshoe prior*. I show that the gamma horseshoe prior results in a prior distribution of the state variances that allows significantly more probability mass near zero than directly placing horseshoe priors on the state variances and hence offers stronger shrinkage while retaining a heavy tail for flexibility. Dynamic structure of the local shrinkage parameter as in Kowal et al. (2019) can be easily added to the gamma horseshoe prior to produce a dynamic version.

Estimating the TVP model with the gamma horseshoe prior can be challenging due to the high dependence between the the latent states and their time-varying variances. A standard Gibbs sampler applied to this TVP model produces posterior draws of model parameters that are slow to converge and mix poorly. To boost sampling efficiency, the ancilarity-sufficiency interweaving strategy (ASIS) of Yu and Meng (2011) is adopted in this paper. A straightforward implementation of the ASIS, however, involves repeated large-scale matrix operations within each MCMC iteration and would be impractical in realistic applications. I develop an alternative MCMC scheme that avoids repeated large-scale matrix operations and instead breaks the parameters of the state variances into blocks and apply the ASIS to each block in a component-wise fashion. The resulting sampler is efficient and computationally tractable. With the use of the horseshoe prior, an advantage of the proposed gamma horseshoe prior is that few user-specified hyper-parameter or manual intervention is needed and hence allows for convenient automated model estimation.

For evaluating out-of-sample forecast performance, the Kalman filter is used conditional on simulations of relevant parameters to approximate the one-step-ahead predictive likelihood. A similar strategy was used in Bitto and Fruhwirth-Schnatter (2019) for the random walk TVP model with homoskedastic latent states and found that the resulting estimate of the one-step-ahead predictive likelihood tends to be more accurate than a pure simulation-based approximation.

The proposed approach is investigated in two applications. In a simulation study where the regression coefficients of the data generating process include both constants, continuous and discrete parameter shifts and their episodical combinations, the in-sample estimation

accuracy of the coefficients under the gamma horseshoe priors is found to significantly outperform the horseshoe prior and be comparable to that under the dynamic horseshoe prior of Kowal et al. (2019). In contrast to the horseshoe prior, the benefit of adding an autoregressive structure to the local parameters is diminished in the gamma horseshoe prior. It is also found that posterior draws of the regression coefficients from the gamma horseshoe prior mix better than those from the dynamic horseshoe prior.

In an empirical illustration, the TVP model is applied to forecast quarterly U.S. inflation rates. The regressors include autoregressive lags and lagged interest rate and unemployment rate. Model estimates based on the gamma horseshoe prior, the horseshoe prior and their dynamic versions are compared. Similar to the findings in the simulation study, posterior draws of the regression coefficients based on the gamma horseshoe prior exhibit better mixing behavior than those from the dynamic horseshoe prior. In out-of-sample forecasts, the gamma horseshoe prior outperforms its dynamic version, the horseshoe prior and the dynamic horseshoe prior based on log predictive likelihoods.

The remainder of the paper is organized as follows. Section 2 provides the details of the TVP model and the shrinkage priors. Estimation details are provided in Section 3. Section 4 and 5 present the simulation study and the empirical application respectively. Section 6 concludes. Additional details of the shrinkage priors and estimation algorithm are provided in appendices.

2 The Model

The TVP model under study is a linear regression model where the regression coefficients follow independent random walk processes:

$$\begin{aligned} y_t &= x_t'\beta_t + \epsilon_t, \quad \epsilon_t \sim N(0, \sigma_t^2), \\ \beta_t &= \beta_{t-1} + \eta_t, \quad \eta_t \sim N(0, \text{diag}(w_t)), \\ \beta_0 &\sim N(0, \text{diag}(w_0)) \end{aligned} \tag{1}$$

where y_t is a scalar dependent variable, x_t is a K-dimensional vector of regressors, β_t is the corresponding time-varying coefficients and $\text{diag}(w_t)$ is a diagonal matrix with the K-by-1 vector w_t in its diagonal for $t = 1, 2, ..., n$. The initial value β_0 plays the role of fixed

regression coefficients[4] and follows a zero-mean normal distribution with the covariance matrix diag(w_0).

Viewed as a state space system, ϵ_t and η_t are the Gaussian disturbances in the measurement and state equations respectively. For economic time series, the measurement equation disturbance ϵ_t is often allowed to have a time dependent variance. In empirical studies of this paper, I use the stochastic volatility (SV) specification for the measurement equation variance σ_t^2:

$$\log(\sigma_t^2) = (1-\rho)\mu + \rho \log(\sigma_{t-1}^2) + \epsilon_{y,t}, \quad \epsilon_{y,t} \sim N(0, \sigma_y^2), \tag{2}$$

where $\log(\sigma_1^2) \sim N(\mu, \sigma_y^2/(1-\rho^2))$. The homoskedastic case can be accommodated by imposing $\sigma_t^2 = \sigma^2$.

The state variance w_t is allowed to be time dependent. Different types of time variations in the regression coefficients β_t can be captured by varying the value of w_t. For example, a constant non-zero value $w_t = w$ leads to the commonly used homoskedastic specification of TVP models (Bitto and Fruhwirth-Schnatter (2019)). The change-point specification that assumes discrete shifts in the regression coefficients can be accommodated by setting $w_t > 0$ at the break points while $w_t = 0$ at other times. Constant regression coefficients can be accommodated by $w_t = 0$ for $t = 1, 2, ..., n$. As argued in Hauzenberger et al. (2020), time variations in TVP models often occur only episodically and only for a subset of the regression coefficients in economic time series data. Such empirical patterns amount to episodical combinations of constant and time-varying parameters, which can be easily accommodated in the TVP model of Equation (1).

2.1 Prior for State Variance

The key parameter in the TVP model of Equation (1) is the state variance w_t. In a Bayesian framework, the task is to develop a suitable prior for w_t that should, on one hand, allow significant likelihoods for w_t close to zero to reduce the risk of overfitting and, on the other hand, contain a heavy tail for w_t to retrieve possible local signals of each time t. Recent developments in the field of Bayesian shrinkage priors provide an

[4]To see this, let $\beta_t^* = \beta_t$ - β_0. The TVP model can be rewritten as $y_t = x_t'\beta_0 + x_t'\beta_t^* + \epsilon_t$, $\beta_t^* = \beta_{t-1}^*$ + η_t and $\beta_0^* = 0$.

ideal toolkit for this task. In this paper, I focus on the horseshoe prior (Carvalho et al. (2010), Polson and Scott (2012)) that is computationally convenient and has shown good performance in many applications (Bhadra et al. (2019))[5].

A straightforward approach would be to directly impose a horseshoe prior on the differenced latent states $\Delta\beta_{j,t} = \beta_{j,t} - \beta_{j,t-1}$ for $j = 1, 2, ..., K$. That amounts to specify $w_{j,t} = r_j s_{j,t}$ with the "global"parameter r_j and the "local" parameter $s_{j,t} \sim IB(0.5, 0.5)$ where IB denotes an inverted beta distribution[6]. In practice for TVP models, the global parameter r_j is often specified as the product of two sub-components $r_j = \tilde{r}_0\tilde{r}_j$ to separate shrinkage at the overall level and at the regressor-specific level, where both $\tilde{r}_0$ and $\tilde{r}_j$ follow $IB(0.5, 0.5)$. This is the "static horseshoe" specification investigated in recent studies such as Kowal et al. (2019) and Huber and Pfarrhofer (2021).

To improve the shrinkage property of the prior for w_t, this paper considers an alternative that translates such a variance shrinkage problem into a variable shrinkage one in a (conditionally) linear regression model by reparameterization. To motivate the prior specification for the state variance w_t, let $\eta_t^* = \text{diag}(\frac{1}{\tilde{w}_t})\eta_t$ denote the normalized state disturbance where $\tilde{w}_t = \pm\sqrt{w_t}$ is the signed square root of the state variance w_t. Substituting the normalized state disturbance η_t^* into the TVP model of Equation (1) gives:

$$\begin{aligned} y_t &= x_t'\beta_0 + \tilde{x}_t'\tilde{w} + \epsilon_t, \\ \eta_t^* &\sim N(0, I_K) \end{aligned} \tag{3}$$

where $\tilde{x}_t$ is a nK-by-1 vector with the first tK elements being $x_t \odot \eta_1^*$, $x_t \odot \eta_2^*$, ..., $x_t \odot \eta_t^*$ and the remaining elements being zero. The notation $\odot$ denotes the element-wise product of matrices of the same size. $\tilde{w} = [\tilde{w}_1, \tilde{w}_2, ..., \tilde{w}_n]$ is a nK-by-1 vector stacking the signed square roots of the state variances w_1, ..., w_n. Equation (3) is the "non-centered" parametrization of the TVP model of Equation (1) in the spirit of Fruhwirth-Schnatter and Wagner (2010).

[5]Alternative shrinkage priors for linear regressions include the spike-and-slab one (George and McCulloch (1993), Ishwaran and Rao (2005)) and the normal-gamma one (Griffin and Brown (2010)) etc. A comprehensive comparison of the various shrinkage priors in the current TVP context is left for future research.

[6]The density of an inverted beta distribution $IB(a, b)$ is $p(x) = \frac{x^{a-1}(1+x)^{-a-b}}{B(a,b)} I\{x > 0\}$ where $B(\cdot, \cdot)$ is the beta function and a and b are positive real numbers. If $x \sim IB(0.5, 0.5)$, then $\sqrt{x} \sim C^+(0, 1)$ and vice versa, where $C^+(0, 1)$ is a standard half-Cauchy distribution with the density $p(z) = \frac{2}{\pi(1+z^2)} I\{z > 0\}$.

Conditional on the normalized state disturbance η_t^*, the measurement equation in the reparametrized TVP model of Equation (3) becomes a linear regression model with the signed square roots $\tilde{w}$ being the fixed coefficients. Hence the task of specifying a shrinkage prior for the variance parameter w_t is transformed into one of placing a shrinkage prior on fixed coefficients of a linear regression, which connects with the rich literature on variable selection in linear regression models. Indeed the horseshoe prior was originally proposed for shrinking fixed coefficients in a linear regression form.

With these considerations, I specify a hierarchical prior for the signed square roots $\tilde{w}$ as $\tilde{w}_{j,t}|v_j, d_{j,t} \sim N(0, v_j d_{j,t})$ with the global parameter v_j and the local parameter $d_{j,t} \sim IB(0.5, 0.5)$ for $j = 1, ..., K$ and $t = 1, ..., n$. The resulting prior for the state variance is a gamma distribution $w_{j,t}|v_j, d_{j,t} \sim G(0.5, 2v_j d_{j,t})$[7].

The remaining piece is to specify the prior for the global parameter v_j. Again I use the fact that the signed square root $\tilde{v}_j = \pm\sqrt{v_j}$ is the fixed coefficient in a conditionally linear regression model by reparametrizing the TVP model of Equation (1):

$$\begin{aligned} y_t &= x_t'\beta_0 + (x_t \odot \beta_t^*)'\tilde{v} + \epsilon_t, \\ \beta_t^* &\sim N(\beta_{t-1}^*, \text{diag}(\phi_t)), \\ \beta_0^* &= 0 \end{aligned} \tag{4}$$

where the transformed latent state is $\beta_{j,t}^* = (\beta_{j,t} - \beta_{j,0})/\tilde{v}_j$, the *scaled state variance* is $\phi_{j,t} = \frac{w_{j,t}}{v_j}$, $\beta_t^* = [\beta_{1,t}^*, \beta_{2,t}^*, ..., \beta_{K,t}^*]$, $\phi_t = [\phi_{1,t}, \phi_{2,t}, ..., \phi_{K,t}]$ and $\tilde{v} = [\tilde{v}_1, \tilde{v}_2, ..., \tilde{v}_K]$. A horseshoe prior for the fixed coefficients $\tilde{v}$ results in $\tilde{v}_j|\tau_0, \tau_j \sim N(0, \tau_0\tau_j)$ with the common component $\tau_0 \sim IB(0.5, 0.5)$ and the individual component $\tau_j \sim IB(0.5, 0.5)$. The equivalent prior for the global parameter $v_j = \tilde{v}_j^2$ is $v_j|\tau_0, \tau_j \sim G(0.5, 2\tau_0\tau_j)$ for $j = 1, ..., K$.

In summary, the proposed prior for the state variance w_t is $w_{j,t}|v_j, d_{j,t} \sim G(0.5, 2v_j d_{j,t})$ with $d_{j,t} \sim IB(0.5, 0.5)$, $v_j|\tau_0, \tau_j \sim G(0.5, 2\tau_0\tau_j)$, $\tau_0 \sim IB(0.5, 0.5)$ and $\tau_j \sim IB(0.5, 0.5)$ for $j = 1, ..., K$ and $t = 1, ..., n$. I label this prior as a *gamma horseshoe* (GHS) prior since the local parameter $d_{j,t}$ follows an inverted beta distribution as in a horseshoe prior while the global parameter v_j follows a gamma distribution conditionally. A dynamic version of the GHS prior in the vein of Kowal et al. (2019) can be easily incorporated by specifying

[7] If $\pm\sqrt{x} \sim N(0, a)$, then $x \sim G(0.5, 2a)$ and vice versa, where the gamma distribution $G(\alpha, \beta)$ has the density $\frac{1}{\Gamma(\alpha)\beta^\alpha} x^{\alpha-1}\exp(-\frac{x}{\beta})$.

$d_{j,t} = d_{j,t-1}^{\rho_j} e_{j,t}$ where $d_{j,0} = 1$, ρ_j is the autoregressive coefficient and $e_{j,t} \sim IB(0.5, 0.5)$ captures the serially uncorrelated component of $d_{j,t}$. I will refer to the dynamic version as the dynamic gamma horseshoe (DGHS) prior to differentiate from the static one with $\rho_j = 0$.

To facilitate comparing the shrinkage priors for TVP models with heteroskedastic latent states, I use the framework of Equation (1) and write the priors in a common global-local format $w_{j,t} = v_j \phi_{j,t}$. The static horseshoe (HS) prior amounts to specify $v_j = \tau_0 \tau_j$ and $\phi_{j,t} = d_{j,t}$ with both τ_0, τ_j and $d_{j,t}$ following $IB(0.5, 0.5)$, while the GHS prior introduces a hierarchical structure $v_j | \tau_0, \tau_j \sim G(0.5, 2\tau_0 \tau_j)$ and $\phi_{j,t} | v_j, d_{j,t} \sim G(0.5, 2d_{j,t})$, adding an extra layer of gamma distributions for both the global and local parameters. A similar comparison can be made between the dynamic horseshoe (DHS) prior and the DGHS prior by letting the variable $d_{j,t} = d_{j,t-1}^{\rho_j} e_{j,t}$ be serially correlated.

2.1.1 Comparing GHS and HS priors

Consider the simplified case that sets the global parameter $v_j = 1$ with $\Delta\beta_{j,t} \sim N(0, w_{j,t})$ and $w_{j,t} = \phi_{j,t}$ where $\phi_{j,t} \sim IB(0.5, 0.5)$ for the HS prior and $\phi_{j,t} | d_{j,t} \sim G(0.5, 2d_{j,t})$, $d_{j,t} \sim IB(0.5, 0.5)$ for the GHS prior.

Based on Cadonna et al. (2020), it can be shown that the marginal density of the local variance $\phi_{j,t}$ under the GHS prior has the following form:

$$p_G(\phi_{j,t}) = \frac{1}{\pi\sqrt{2\pi}} \, \phi_{j,t}^{-\frac{1}{2}} \, \mathcal{U}\left(1, 1, \frac{\phi_{j,t}}{2}\right)$$

where $\mathcal{U}$ denotes the confluent hyper-geometric function of the second kind. The limiting behavior of $\phi_{j,t}$ can be described as follows (Abramowitz and Stegun (1973), Cadonna et al. (2020)):

$$\begin{aligned} p_G(\phi_{j,t}) &= \frac{1}{\pi\sqrt{2\pi}} \, \phi_{j,t}^{-\frac{1}{2}} (-\log\phi_{j,t} + \log 2 + \gamma) + \mathcal{O}\left(\sqrt{\phi_{j,t}} \log\phi_{j,t}\right) \quad \text{as} \quad \phi_{j,t} \to 0 \\ p_G(\phi_{j,t}) &= \frac{\sqrt{2}}{\pi\sqrt{\pi}} \, \phi_{j,t}^{-\frac{3}{2}} \left(1 + \mathcal{O}\left(\frac{1}{\phi_{j,t}}\right)\right) \quad \text{as} \quad \phi_{j,t} \to \infty \end{aligned} \tag{5}$$

where γ is the Euler's constant. It is clear from Equation (5) that $p(\phi_{j,t})$ under the GHS prior goes to infinity at the point 0 and has a power-law tail, thus showing a similar shape as the HS prior. To compare their difference, the following results can be established about

the density ratio $r(\phi_{j,t}) = \frac{p_G(\phi_{j,t})}{p_H(\phi_{j,t})}$ where $p_H(\phi_{j,t}) = \frac{1}{\pi}\phi_{j,t}^{-\frac{1}{2}}(1+\phi_{j,t})^{-1}$ is the density of $\phi_{j,t}$ under the HS prior:

$$r(\phi_{j,t}) = \frac{1}{\sqrt{2\pi}}\,(1+\phi_{j,t})(-\log\phi_{j,t} + \log 2 + \gamma) + \mathcal{O}\left(\phi_{j,t}^2 \log\phi_{j,t}\right) \quad \text{as} \quad \phi_{j,t} \to 0$$
$$r(\phi_{j,t}) = \sqrt{\frac{2}{\pi}}\,\frac{1+\phi_{j,t}}{\phi_{j,t}}\left(1 + \mathcal{O}\left(\frac{1}{\phi_{j,t}}\right)\right) \quad \text{as} \quad \phi_{j,t} \to \infty \tag{6}$$

From Equation (6), the density ratio $r(\phi_{j,t})$ goes to infinity at the point 0, showing that the GHS prior offers stronger shrinkage than the HS prior. At the same time, the tail of $p_G(\phi_{j,t})$ decays at the same speed as $p_H(\phi_{j,t})$ and avoids the risk of "over-shrinking" by the GHS prior.

Following Carvalho et al. (2010), I also compare the shrinkage properties of the GHS and HS priors by the shrinkage parameter $\kappa_{j,t} = \frac{1}{1+\phi_{j,t}}$ where $\kappa_{j,t} \to 1$ implies shrinking $\Delta\beta_{j,t}$ towards zero while $\kappa_{j,t} \to 0$ implies minimal shrinkage for $\Delta\beta_{j,t}$. Using the change-of-variable formula, it can be derived that under the HS prior, $\kappa_{j,t} \sim Beta(0.5, 0.5)$ and hence its density has a symmetric "U" shape. For the GHS prior, the marginal density of $\kappa_{j,t}$ is:

$$p_G(\kappa_{j,t}) = 2^{-\frac{1}{2}}\pi^{-\frac{3}{2}}\,\kappa_{j,t}^{-\frac{3}{2}}\,(1-\kappa_{j,t})^{-\frac{1}{2}}\,\mathcal{U}\left(1, 1, \frac{1-\kappa_{j,t}}{2\kappa_{j,t}}\right)$$

Figure 1 compares the marginal density of $\kappa_{j,t}$ under the HS and GHS priors. The density of $\kappa_{j,t}$ under the GHS prior has a "U" shape that is tilted towards the end $\kappa_{j,t} = 1$. The density mass of $\kappa_{j,t}$ under the GHS prior that is located in the two tail regions $(0, 0.1)$ and $(0.9, 1)$ is 16% and 37% respectively while the corresponding density mass is 21% and 21% for $\kappa_{j,t}$ under the HS prior. Therefore the GHS prior allocates more probability mass towards the end of complete shrinkage $\kappa_{j,t} \approx 1$ than the HS prior without much reduction in its probability mass at the other end of minimal shrinkage $\kappa_{j,t} \approx 0$. I also compare the conditional density of $\kappa_{j,t}$ under the HS and GHS priors based on the hierarchical representation of inverted beta distributions in Makalic and Schmidt (2016) and reach similar findings favoring the GHS prior. The details of comparing the conditional density of $\kappa_{j,t}$ are provided in Appendix A.

To further alleviate the concern of over-shrinking by the GHS prior, the density of $\Delta\beta_{j,t}$ under the simplified HS and GHS priors is compared based on a million simulations. Checking the two tail regions of $\Delta\beta_{j,t}$: $(-\infty, -25) \cup (25, \infty)$ and $(-\infty, -100) \cup (100, \infty)$, the

density mass of $\Delta\beta_{j,t}$ in these regions under the GHS prior is 1.6% and 0.4% respectively, which is slightly lower than under the HS prior (2.0% and 0.5% respectively) but remains appreciable to accommodate extreme values of $\Delta\beta_{j,t}$.

2.2 Prior for Other Model Parameters

Besides the state variance w_t, other parameters in the TVP model of Equation (1) include the measurement equation variance σ_t^2 and the initial state β_0.

For the SV specification of the measurement equation variance σ_t^2 (Equation (2)), the priors are $\mu \sim N(0, 10)$, $\rho \sim N(0.95, 0.04)I_{\{-1<\rho<1\}}$. Note that an informative prior is used for the autoregressive coefficient ρ to reflect the empirical regularity that the volatility of economic time series tends to be highly persistent. For the variance parameter σ_y^2 in the SV model, I follow Kastner and Fruhwirth-Schnatter (2014) and specify a Gaussian prior for its signed square root $\tilde{\sigma}_y = \pm\sqrt{\sigma_y^2}$ as $\tilde{\sigma}_y|s_y \sim N(0, s_y)$ to facilitate estimation. It is possible to specify a fixed number (e.g. 1) for the hyper-parameter s_y as in Kastner and Fruhwirth-Schnatter (2014). Considering that finding an appropriate fixed value for s_y is not obvious in general, I place a prior $s_y \sim IB(0.5, 0.5)$ in this paper to determine s_y in a data-driven way. As will be shown in Section 3, sampling s_y under the $IB(0.5, 0.5)$ prior is from closed-form distributions and is convenient. The impact of placing a prior for s_y is analyzed in Appendix B in the context of the empirical study of this paper.

In the case where the measurement equation disturbance is homoskedastic $\sigma_t^2 = \sigma^2$, the Jeffery's prior $\sigma^2 \propto \frac{1}{\sigma^2}$ is used.

For the initial state β_0, a horseshoe prior is imposed to push insignificant elements towards zero. Specifically $\beta_{j,0}|\tau_{0,0}, \tau_{j,0} \sim N(0, \tau_{0,0}\tau_{j,0})$ with $\tau_{0,0} \sim IB(0.5, 0.5)$ and $\tau_{j,0} \sim IB(0.5, 0.5)$ for $j = 1, ..., K$.

3 Estimation

Given the priors described in Section 2, a standard Gibbs sampler can be developed for estimating the TVP model of Equation (1). However the resulting posterior draws suffer

from slow convergence and poor mixing, particularly when the state variances are close to zero. In this paper, I adopt the ancillarity-sufficiency interweaving strategy (ASIS) of Yu and Meng (2011) to design a more efficient Gibbs sampler. The ASIS boosting strategy has shown good performance in many applications of state space models (e.g. Simpson et al. (2017) and Bitto and Fruhwirth-Schnatter (2019)). A discussion of applying the ASIS is provided in Section 3.1. The details of the proposed Gibbs sampler are presented in Section 3.2.

3.1 ASIS Boosting

The ASIS considers two parametrizations of a hierarchical latent variable model: a sufficient augmentation (SA) in which the latent variable is a sufficient statistic for the relevant parameters, and an ancillary augmentation (AA) in which the same parameters are all in the distribution of the observation and hence the latent variable is an ancillary statistic for them. By moving between a SA-AA pair, Yu and Meng (2011) found that the resulting Markov chain Monte Carlo (MCMC) algorithm is often more efficient and, under certain conditions, provides the fastest converging algorithm within a general class of data augmentation schemes.

The ASIS can be implemented in a component-wise fashion. That is, a *conditional* SA-AA pair for a subset of model parameters can be formed by treating other parameters as fixed, while the conditional SA-AA pair can be different for different subsets of model parameters. Hence the ASIS is quite flexible for use in practical applications.

For the TVP model of Equation (1), the key to implementing the ASIS is to find a suitable (conditional) SA-AA pair or SA-AA pairs of model parametrizations for the parameters that are difficult to estimate in a vanilla Gibbs sampler, namely, the state variances and associated hyper-parameters.

Return to the TVP model of Equation (1). It is clear that the latent state β_t is a sufficient statistic for the state variance w_t and for that matter the signed square root $\tilde{w}_t$. Since the reparametrization of Equation (3) moves the signed square roots $\tilde{w}$ to the measurement equation and leaves the new latent state η_t^* free of $\tilde{w}_t$, one may be tempted to directly apply the ASIS to the signed square roots $\tilde{w}$ by treating Equation (1) and Equation

(3) as a SA-AA pair. The drawback of this strategy however is that drawing the signed square roots $\tilde{w}$ in Equation (3) will be working with an enormous linear regression with nK regressors. Even with the state-of-art algorithm in Bhattacharya et al. (2016), the computational complexity is in the order of $\mathcal{O}(n^3K)$ in each MCMC iteration and could be overwhelming in typical economic studies with hundreds of data points[8].

This paper proposes an alternative strategy to avoid repeated large-scale matrix operations while boosting the sampling quality. Instead of directly boosting the state variance, two separate component-wise ASISs are applied to the global parameter v_j and the local parameter $d_{j,t}$ in the prior of the state variance.

Recall from Equation (4) the auxiliary variable of the scaled state variance $\phi_{j,t} = \frac{w_{j,t}}{v_j}$. It follows $w_{j,t} = v_j\phi_{j,t}$ with $\phi_{j,t}|v_j, d_{j,t} \sim G(0.5, 2d_{j,t})$. Conditional on the scaled state variance $\phi_{j,t}$, the latent state $\beta_{j,t}$ is a sufficient statistic for the global parameter v_j and hence the TVP model of Equation (1) can be viewed as a SA representation for v_j. On the other hand, the reparametrization of Equation (4) has the signed squared root $\tilde{v}_j$ of the global parameter v_j in its measurement equation, while its state equation $\beta^*_{j,t} \sim N(\beta^*_{j,t-1}, \phi_{j,t})$ is conditionally free of the global parameter v_j. Therefore the reparametrization of Equation (4) constitutes a conditional AA representation for v_j. An ASIS boosting for the global parameter v_j can be conducted based on this conditional SA-AA pair.

For the local parameter $d_{j,t}$, consider the subset of Equation (4) along with the conditional distribution of the scaled state variance $\phi_{j,t}$:

$$\begin{aligned} \Delta\beta^*_{j,t} &= \beta^*_{j,t} - \beta^*_{j,t-1} \sim N(0, \phi_{j,t}) \\ \phi_{j,t}|v_j, d_{j,t} &\sim G(0.5, 2d_{j,t}) \end{aligned} \tag{7}$$

Equation (7) can be viewed as a nested latent variable model with $\Delta\beta^*_{j,t}$ being the observation, $\phi_{j,t}$ being the latent variable and $d_{j,t}$ being the parameter of interest. In this nested model, the latent variable $\phi_{j,t}$ is a sufficient statistic for $d_{j,t}$ while the observation $\Delta\beta^*_{j,t}$ is independent of $d_{j,t}$ conditional on $\phi_{j,t}$. Hence Equation (7) constitutes a conditional SA representation for $d_{j,t}$. Now let $\phi^*_{j,t} = \frac{\phi_{j,t}}{d_{j,t}}$. It follows that the conditional distribution $\phi^*_{j,t}|v_j, d_{j,t} \sim G(0.5, 2)$ is free of $d_{j,t}$. Substituting $\phi_{j,t} = \phi^*_{j,t}d_{j,t}$ into Equation (7) gives a

[8]See Johndrow et al. (2020) and Hauzenberger et al. (2020) for methods that use approximations to the exact algorithm of Bhattacharya et al. (2016).

conditional AA representation for $d_{j,t}$:

$$\begin{aligned}\Delta\beta^*_{j,t} &\sim N(0, \phi^*_{j,t} d_{j,t}) \\ \phi^*_{j,t}|v_j, d_{j,t} &\sim G(0.5, 2)\end{aligned} \tag{8}$$

A second ASIS boosting can be applied to this conditional SA-AA pair for the local parameter $d_{j,t}$.

3.2 MCMC Estimation

The proposed Gibbs sampler divides the model parameters into the following blocks:

1. Measurement equation variance:
   (a) SV specification: σ_t^2, μ, ρ, σ_y^2 and associated hyper-parameters including s_y,
   (b) Homoskedastic specification: σ^2,
2. Hyper-parameters $\{\tau_0, \tau_j\}$ and $\{\tau_{0,0}, \tau_{j,0}\}$ for the global parameter v_j and the initial state $\beta_{j,0}$ respectively,
3. Hyper-parameters for the local parameter $d_{j,t}$,
4. Transformed latent states $\beta^*_{j,t}$, global parameter v_j and initial state β_0,
5. Scaled state variance $\phi_{j,t}$ and local parameter $d_{j,t}$,

where $j = 1, 2, ..., K$ and $t = 1, 2, ..., n$.

In block 1, sampling of the measurement equation variance in the SV specification is similar to Kastner and Fruhwirth-Schnatter (2014) by adopting the log linearization strategy of Kim et al. (1998) and Omori et al. (2007). The details are given in Appendix B. In the homoskedastic case $\sigma_t^2 = \sigma^2$ with the Jeffery's prior $\sigma^2 \propto \frac{1}{\sigma^2}$, the posterior is $\sigma^2|y, x, \beta \sim \text{IG}\left(\frac{n}{2}, \frac{1}{2}\sum_{t=1}^n \epsilon_t^2\right)$ where $\epsilon_t = y_t - x_t'\beta_t$, $y = [y_1, ..., y_n]$, $x = [x_1, ..., x_n]$, $\beta = [\beta_1, ..., \beta_n]$ and IG denotes the inverse gamma distribution.

Block 2 is the hyper-parameters for two horseshoe priors. By adopting the hierarchical inverse gamma representation of Makalic and Schmidt (2016), the posteriors of these hyper-parameters are inverse gamma distributions. Appendix C provides the details.

Block 3 contains the hyper-parameters for the local parameter $d_{j,t}$. In the static case, an auxiliary variable $e_{j,t}$ is introduced to represent $d_{j,t} \sim IB(0.5, 0.5)$ as a hierarchical inverse gamma distribution $d_{j,t} \sim IG\left(0.5, \frac{1}{e_{j,t}}\right)$ and $e_{j,t} \sim IG(0.5, 1)$(Makalic and Schmidt (2016)). The posterior for the auxiliary variable is $e_{j,t}|d_{j,t} \sim IG\left(1, 1 + \frac{1}{d_{j,t}}\right)$. In the dynamic case, use the log linearization $\log(d_{j,t}) = \rho_j \log(d_{j,t-1}) + \log(\xi_{j,t})$ where $\xi_{j,t} \sim IB(0.5, 0.5)$. Following Polson et al. (2013) and Kowal et al. (2019), $\log(\xi_{j,t})$ can be represented as a precision mixture of normals $\log(\xi_{j,t}) \sim N\left(0, \frac{1}{e_{j,t}}\right)$, where $e_{j,t} \sim PG(1, 0)$ is an auxiliary variable and PG denotes the polya-gamma distribution (Barndorff-Nielsen et al. (1982)). The posteriors of the parameters ρ_j and $e_{j,t}$ are derived in Appendix E.

Block 4 and 5 implement two component-wise ASISs. For block 4, the steps are as follows:

i Conditional on ϕ_t, β_0, $\tilde{v}$ and σ_t^2, draw the transformed latent states β_t^* from the AA represention (Equation (4)) by the simulation smoother of Durbin and Koopman (2002)[9].

ii Let α be a $2K$-by-1 vector stacking β_0 and $\tilde{v}$. Conditional on β_t^*, σ_t^2 and the hyper-parameters in block 2, draw α from a linear regression with the posterior $N(b, B)$, where $B^{-1} = B_0^{-1} + \sum_{t=1}^n \frac{1}{\sigma_t^2} \tilde{x}_t \tilde{x}_t'$, $B^{-1}b = \sum_{t=1}^n \frac{1}{\sigma_t^2} \tilde{x}_t y_t$, B_0 is a diagonal matrix with the diagonal elements $\tau_{0,0}\tau_{1,0}$, ..., $\tau_{0,0}\tau_{K,0}$, $\tau_0\tau_1$, ..., $\tau_0\tau_K$, and $\tilde{x}_t = [x_t, x_t \odot \beta_t^*]'$.

iii Keep the sign of $\tilde{v}$. Calculate the latent state $\beta_{j,t} = \beta_{j,0} + \tilde{v}_j \beta_{j,t}^*$ of the SA representation (Equation (1)).

iv Update v and β_0 in the SA representation of Equation (1). It is possible to use a nested Gibbs sampler to alternate updating v and β_0. In this paper, I marginalize over β_0 when updating v to improve sampling efficiency. The details are provided in Appendix D.

v Update $\tilde{v}_j$ as the positive square root of v_j times the sign from Step iii. Update the transformed latent state $\beta_{j,t}^* = \frac{\beta_{j,t} - \beta_{j,0}}{\tilde{v}_j}$.

[9]Alternative approaches to simulate the latent states from a linear Gaussian state space system include Fruhwirth-Schnatter (1994), Rue (2001) and McCausland et al. (2011) etc.

Sampling the parameters of block 5 has the following steps:

i Draw the transformed latent variable $\phi^*_{j,t} = \frac{\phi_{j,t}}{d_{j,t}}$ in the AA representation of Equation (8):

$$\phi^*_{j,t}|d_{j,t}, \beta^*_{j,t} \sim GIG\left(0, 1, \frac{\left(\Delta\beta^*_{j,t}\right)^2}{d_{j,t}}\right)$$

ii Based on the AA representation of Equation (8), draw

$$d_{j,t}|e_{j,t}, \phi^*_{j,t}, \beta^*_{j,t} \sim IG\left(1, \frac{1}{e_{j,t}} + \frac{1}{2\phi^*_{j,t}}\left(\Delta\beta^*_{j,t}\right)^2\right)$$

in the static case. In the dynamic case, draw $d_{j,t}$ based on the algorithm in Kowal et al. (2019). The key is to treat $d_{j,t}$ as the stochastic volatility of a SV model and use the log linearization strategy of Kim et al. (1998) and Omori et al. (2007) to sample $\log(d_{j,t})$. The details are given in Appendix E.

iii Compute the latent variable $\phi_{j,t} = \phi^*_{j,t} d_{j,t}$ for the SA representation of Equation (7).

iv Based on the SA representation of Equation (7), update $d_{j,t}$ from the following posterior in the static case:

$$d_{j,t}|e_{j,t}, \phi_{j,t} \sim IG\left(1, \frac{1}{e_{j,t}} + \frac{\phi_{j,t}}{2}\right)$$

In the dynamic case, update $d_{j,t}$ based on the algorithm in Kowal et al. (2019) with the details in Appendix E.

v Update the transformed latent variable $\phi^*_{j,t} = \frac{\phi_{j,t}}{d_{j,t}}$.

This completes the description of the MCMC algorithm for estimating the TVP model with the proposed gamma horseshoe priors. It should be noted that the proposed algorithm mostly samples from closed-form distributions and scales linearly with the number of observations n and the number of regressors K. No manual intervention or difficult user-specified hyper-parameters are required. Thus model estimation can be performed efficiently in an automated fashion and facilitates practical applications.

3.3 Predictive Likelihoods

In this paper, the predictive likelihood is used to compare different prior specifications of TVP models. See Geweke and Amisano (2010) for a review of Bayesian predictive analysis. Specifically, given a model specification $\mathcal{M}$ and a data sample of the dependent variable $y^n = \{y_t\}_{t=1}^n$ and regressors $x^{n+1} = \{x_t\}_{t=1}^{n+1}$, the one-step-ahead predictive likelihood is $p(y_{n+1}|y^n, x^{n+1}, \mathcal{M})$ that integrates out all the parameters in model $\mathcal{M}$. For expositional convenience, the regressors in x_t are treated as exogenous. It should be understood that in the case of predictive regressions, x_t are variables observed at time $t-1$.

To compute the one-step-ahead predictive likelihood $p(y_{n+1}|y^n, x^{n+1}, \mathcal{M})$, I use the strategy that is labeled as the *conditionally optimal Kalman mixture approximation* in Bitto and Fruhwirth-Schnatter (2019). Let θ^n collect the parameters $\{w_t\}_{t=1}^n$, $\{\sigma_t^2\}_{t=1}^n$ and other model hyper-parameters. It is straightforward to derive the conditional distribution:

$$y_{n+1}|x_{n+1}, w_{n+1}, \sigma_{n+1}^2, b_n, B_n \sim N\left(x_{n+1}' b_n,\ \sigma_{n+1}^2 + x_{n+1}' \left(B_n + \text{diag}(w_{n+1})\right) x_{n+1}\right) \tag{9}$$

where b_n and B_n are the mean and covariance matrix of the filtering distribution $\beta_n|y^n, x^n, \theta^n \sim N(b_n, B_n)$. One can approximate the one-step-ahead predictive likelihood as:

$$p\left(y_{n+1}|y^n, x^{n+1}, \mathcal{M}\right) \approx \frac{1}{M}\sum_{i=1}^{M} p\left(y_{n+1}|x_{n+1}, w_{n+1}^{(i)}, \left(\sigma_{n+1}^2\right)^{(i)}, b_n^{(i)}, B_n^{(i)}\right) \tag{10}$$

where $w_{n+1}^{(i)}$ and $\left(\sigma_{n+1}^2\right)^{(i)}$ are simulated based on posterior draws of the gamma horseshoe prior and the SV model for the measurement equation disturbance. The filtered mean $b_n^{(i)}$ and filtered covariance matrix $B_n^{(i)}$ are computed based on a Kalman filter with their derivations provided in Appendix F.

Given the one-step-ahead predictive likelihood $p(y_t|y^{t-1}, x^t, \mathcal{M})$, the cumulative log predictive likelihood $\sum_{i=1}^m \log p(y_{n+i}|y^{n+i-1}, x^{n+i}, \mathcal{M})$ over a prediction sample $t = n+1, ..., n+m$ is the criterion for comparing the performance of model $\mathcal{M}$ with alternatives.

4 Simulation Study

A sample of 300 data points are simulated from a linear regression model with 6 coefficients exhibiting different types of time variation over $t = 1, ..., 300$:

1 Random walk: $\beta_{1,t} = \sum_{j=1}^{t} u_j$ with $u_j \sim N(0, 0.01)$.

2 Change point: $\beta_{2,t} = I_{\{100<t\leq 200\}} - I_{\{t>200\}}$.

3 Mixture of constant parameter, random walk and change point:

$$\beta_{3,t} = \left(\sum_{j=1}^{t} u_j\right) I_{\{100<t\leq 200\}} + I_{\{t>200\}}$$

with $u_j \sim N(0, 0.01)$.

4 Ones: $\beta_{4,t} = 1$.

5 Small constant: $\beta_{5,t} = 0.1$.

6 Zeros: $\beta_{6,t} = 0$.

The regressors are from standard normal distributions. The dependent variables is generated by adding a noise from $N(0, \sigma^2)$ where σ^2 is calibrated such that the ratio of σ^2 to the variance of the dependent variable is 0.2.[10] The 4 TVP priors (HS, DHS, GHS and DGHS) are applied to the simulated data. In estimation, the measurement equation disturbance is taken to be homoskedastic. A sample of 10,000 posterior draws are kept for analysis after a burn-in of length 5,000.[11]

Figure 2 shows the point-wise posterior medians and 90% credible sets of the regression coefficients estimated by the various TVP priors. The posterior medians match the true coefficients reasonably well. Among the 4 TVP priors, the HS specification leads to markedly more volatile posterior medians and wider credible sets of the coefficient estimates than the other 3 prior specifications, particularly for the constant coefficients. The coefficient estimates of the GHS, DGHS and DHS priors are close with the exception of the change-point coefficient where the DGHS and DHS priors produce sharper estimates of the change points than the GHS prior.

[10] In experiments, another two data generating processes are studied where the ratio of σ^2 to the variance of the dependent variable is 0.5 and 0.8 respectively. The estimation results are qualitatively similar.

[11] Generating 1,000 posterior draws from the GHS and DGHS prior specifications takes about 20 and 26 seconds respectively on a standard desktop computer with a 3.0 GHz Intel Core i5 CPU, running in MATLAB R2020b.

To quantify the accuracy of coefficient estimates from the TVP priors, I compute the point-wise root mean square error (RMSE) for each coefficient j at point t:

$$\text{RMSE}_{j,t} = \sqrt{\frac{1}{M}\sum_{i=1}^{M}\left(\hat{\beta}_{j,t}^{(i)} - \beta_{j,t}\right)^2} \tag{11}$$

where $\hat{\beta}_{j,t}^{(i)}$ denotes a posterior draw of the coefficient from a given model and $\beta_{j,t}$ the true coefficient value. Box plots of the distributions of $\text{RMSE}_{j,t}$ across $t = 1, ..., 300$ for each coefficient $j = 1, ..., 6$ are shown in Figure 3. A concentrated distribution of $\text{RMSE}_{j,t}$ implies a stable level of estimation precision across points t and hence is more desirable.

In Figure 3, the RMSEs from the HS prior clearly lag behind those from the other 3 priors. The DGHS and DHS priors show very similar levels of estimation precision, while the RMSEs of the GHS prior are comparable to those of the DGHS and DHS priors except in the case of the change-point coefficient where the two dynamic priors tend to perform slightly better.

It may appear counter intuitive that the GHS prior performs as well as the DGHS prior as the autoregressive structure in the DGHS prior is more flexible. However this observation ignores that the gamma distributions placed on the global and local components of the GHS and DGHS priors already allows an extra layer of flexibility and hence the autoregressive structure becomes less important than in the case of the HS and DHS priors. To see this, note that, in both the GHS and DGHS priors, the state variance $w_{j,t} = v_j\phi_{j,t}$ can be re-written as $w_{j,t} = v_j d_{j,t}\phi_{j,t}^*$ where $\phi_{j,t}^* = \frac{\phi_{j,t}}{d_{j,t}}$ and $\phi_{j,t}^*|v_j, d_{j,t} \sim G(0.5, 2)$. Hence local behaviors in the GHS and DGHS priors are controlled by two parameters $d_{j,t}$ and $\phi_{j,t}^*$. In contrast, the HS and DHS priors have a single parameter $d_{j,t}$ to adjust local behavior and hence the extra flexibility rendered by an autoregressive structure on $d_{j,t}$ in the DHS prior makes larger difference relative to the HS prior.

In terms of the mixing efficiency of posterior draws, I first show the benefit of the ASIS boosting in Figure 4, which plots the point-wise effective sample size (ESS) of the regression coefficient estimates by the GHS prior with and without the ASIS boosting[12]. ASIS boosting improves the ESS over the standard Gibbs sampler for all coefficients and

[12]The ESS is computed by the initial monotone sequence method of Geyer (1992) and is normalized by dividing by the number of posterior draws.

particularly for the constant ones. Without boosting, the posterior draws for the constant coefficients from a standard Gibbs sampler have extremely low ESSs and are hardly usable for model inference. The computational cost of adding the ASIS steps is minimal, increasing the running time of generating 1,000 posterior draws by about 1 second in this simulation example.

In Figure 5, the ESSs of the regression coefficient estimates by the GHS, DGHS and DHS priors are compared. For clearer exposition, the figures shows the logarithm of the ratio of the point-wise ESSs of the GHS and DGHS priors to those of the DHS prior. The DGHS prior leads to comparable or slightly better mixed posterior draws of the time-varying coefficients than the DHS prior but shows greater sampling efficiency for the constant coefficients. The GHS prior performs the best among the three priors and shows uniformly and significantly higher sampling efficiency for all coefficients. It is noted that, for both the DGHS and DHS priors, posterior draws of the autoregressive coefficients in the dynamic shrinkage process are found to mix unsatisfactorily, which hinders the sampling efficiency of these two dynamic priors.

5 Empirical Illustration

To illustrate the proposed methodology, I apply the TVP model of Equation (1) to forecast the quarterly U.S. inflation rate. The dependent variable is the quarter-to-quarter change of annualized log quarterly inflation rate. The regressors include a constant, lags 1 to 6 of the dependent variable, lagged quarter-to-quarter change of quarterly average 3-month U.S. treasury bill rate, and lagged quarter-to-quarter change of quarterly average U.S. unemployment rate[13]. The data sample runs from Q2 1957 to Q2 2022 with a total of 261 observations. Figure 6 shows the data used in the estimation. The high volatilities in late 1970s and the recent COVID pandemic are evident in the inflation rate data.

MCMC estimation is performed with 20,000 posterior draws after a burn-in of length

[13]The data source is the FRED database of the U.S. federal reserve bank of St. Louis. The series names are CPILFESL, TB3MS and UNRATE for consumer price index, 3-month treasury bill rate and unemployment rate respectively. Quarterly average is computed as the average monthly values within each quarter.

5,000. The SV specification of Equation (2) for the measurement equation variance is used for the TVP model. The time variation patterns of the estimated coefficients are similar across the TVP prior specifications except for the HS prior whose estimates are more volatile than the others. Appendix G provides all the estimated β_t and stochastic variance σ_t^2 by the 4 TVP prior specifications. As an illustration, Figure 7 shows the point-wise posterior medians and 90% credible sets of the coefficients β_t from the GHS prior, along with the OLS estimate for comparison. The intercept shows a small yet prolonged dip in the 1990s. For the autoregressive lags, coefficients on lag 1 and 3 trend upwards while coefficients on lag 2, 4, 5 and 6 decline gradually over time, though the magnitude of changes in the autoregressive coefficients is relatively small. The coefficient on the lagged interest rate variable is markedly smaller than the OLS estimate and contains zero within its 90% credible sets for most of the time periods. For the lagged unemployment rate, its coefficient shows a V shape over the data sample. The V bottom is reached around mid 1970s when the posterior of the coefficient on the lagged unemployment rate mostly falls in the negative region, suggesting a pattern consistent with the Phillips curve. Since then, the posterior median of the coefficient on the lagged unemployment rate steadily goes up towards zero. It is also interesting to note that the spikes of inflation rates in the late 1970s and the COVID pandemic are mostly reflected in the estimated stochastic variance σ_t^2 (the last panel of Figure 7) instead of the time-varying coefficients β_t.

As will be shown in Section 5.1, forecasting performance of the HS prior significantly lags behind the other 3 TVP priors. So I focus on comparing the sampling efficiency of the coefficients β_t by the GHS, DGHS and DHS priors. Similar to the simulation study, Figure 8 shows the logarithm of the ratio of the point-wise ESSs of estimated β_t by the GHS and DGHS priors to those of the DHS prior. Between the pair of DGHS and DHS priors, the ESSs of estimated β_t by the DGHS prior are generally higher than those of the DHS prior, while the GHS prior leads to uniformly higher sampling efficiency for all coefficients than both the DGHS and DHS priors.

5.1 Comparing TVP Priors by Out-of-Sample Forecasts

The TVP priors are evaluated via out-of-sample forecasts. The log predictive likelihoods discussed in Section 3.3 are used to compare the performance of the 4 TVP priors. An iterative prediction exercise is conducted. First the sample from Q2 1957 to Q4 2003 is used to estimate the TVP models under the 4 priors and predictive likelihoods for Q1 2004 are computed. Next the estimation sample is expanded by one observation to include Q1 2004 and generates the forecast for Q2 2004. This procedure is repeated until Q2 2022 with a total of 74 out-of-sample forecasts.

Figure 9 shows the evolution of the difference in the cumulative log predictive likelihoods of the GHS and DGHS priors relative to those of the HS and DHS priors. The dominance of the GHS and DGHS priors in predictive likelihoods over the HS prior is evident to the extent that the difference between the predictive likelihoods of the GHS and DGHS priors is hardly visible in the upper panel of Figure 9. Relative to the DHS prior, the GHS and DGHS priors steadily accumulate gains in predictive likelihoods throughout the forecast sample. The volatile movements of inflation rates during the COVID pandemic appear to result in large predictive gains for the GHS and DGHS priors relative to the DHS prior. Among the two gamma horseshoe priors, the GHS prior performs better than the DGHS prior and shows steady improvement in predictive likelihoods over the forecast sample. These forecast results show the benefits of the GHS prior that has a simpler structure than the dynamic priors yet produces effective shrinkage for the regression coefficients.

As a commonly used gauge of predictive improvement in the forecasting literature, Diebold-Mariano tests (Diebold and Mariano (1995)) are conducted and find that the averages of the log predictive likelihood differences in the GHS-DHS and DGHS-DHS pairs are highly significant with p-values of 0.0007 and 0.0008 respectively. Hence the Diebold-Mariano tests support significant predictive improvement of the gamma horseshoe priors, static or dynamic, over the dynamic horseshoe prior of Kowal et al. (2019). A similar Diebold-Mariano test for the GHS-DGHS pair returns a p-value of 0.04 and provides modest support of the more parsimonious GHS prior specification.

An interesting question is whether the predictive gain of the gamma horseshoe priors is from more accurate prediction of the location of the inflation rate. I focus on the comparison

with the DHS prior. Table 1 shows the mean squared error (MSE) of the predictions under the GHS, DGHS and DHS priors. Given the volatile behavior of inflation rates during the COVID pandemic, the MSE is computed for the entire prediction sample from Q1 2004 to Q2 2022 as well as the pre-pandemic subsample from Q1 2004 to Q4 2019. It is found that the MSEs under the 3 TVP priors are very close in the pre-pandemic subsample, suggesting that during time periods of relatively stable inflation rates, the predictive gain of the gamma horseshoe priors relative to the DHS prior is mostly from capturing the tail regions of the inflation rate distribution. On the other hand, the full-sample MSE of the GHS prior is smaller than the DHS prior, which in turn is smaller than the DGHS prior, supporting better point forecasts of the GHS prior than the two dynamic TVP priors during time periods of volatile inflation rates.

6 Conclusion

The TVP model with time-dependent state variance offers a flexible framework to accommodate a wide variety of time variation patterns of parameter changes but is prone to over-parameterization. Effective shrinkage on the state variance is crucial to reduce the risk of model over-fitting. This paper introduces a hierarchical horseshoe prior named *gamma horseshoe prior* on the state variance that allows for stronger shrinkage than the conventional horseshoe prior while maintaining flexibility to accommodate local signals. The new prior is motivated by reparametrizing the TVP model that translates a variance shrinkage problem into a variable shrinkage one borrowing on the insight from Fruhwirth-Schnatter and Wagner (2010). Dynamic version of the gamma horseshoe prior in the vein of Kowal et al. (2019) is also provided.

An MCMC algorithm is developed to estimate the TVP model under the proposed gamma horseshoe priors that employs the ASIS of Yu and Meng (2011) as the critical ingredient to boost sampling efficiency. The novelty of the algorithm is that it avoids repeated large-scale matrix operations and instead applies the ASIS in a tractable component-wise fashion. In both simulation and an inflation rate forecast exercise, the gamma horseshoe priors are shown to provide effective shrinkage for the regression coefficients of the TVP model. It is also noted that the need for dynamic structure is reduced in the gamma

horseshoe priors relative to the case of the horseshoe priors. In out-of-sample forecasts, the gamma horseshoe prior outperforms the horseshoe prior and their dynamic versions.

Recently Cadonna et al. (2020) proposes a triple gamma prior that generalizes the $IB(0.5, 0.5)$ distribution, which is equivalent to an F distribution $F(1, 1)$, in the horseshoe prior by a general F distribution $F(a_F, b_F)$. Cadonna et al. (2020) shows that when a_F and b_F are below 1, more effective shrinkage can be achieved than the horseshoe prior. Combining the insight from Cadonna et al. (2020) with the idea of the proposed GHS prior could be an interesting extension for dynamic shrinkage of TVP models. Also this paper focuses on the univariate TVP model. Extension to the multivariate case is possible (e.g. the Cholesky decomposition approach introduced in Lopes et al. (2018) and Carriero et al. (2019) that reduces an multivariate TVP model into a system of independent univariate TVP models). Given its computational efficiency, studying the proposed gamma horseshoe prior in the multivariate context could be an interesting venue of future research. Finally theoretical investigations of what classes of data generating processes can be better approximated by the TVP model than other non-parametric approaches could be an important topic that merits further research.

Table 1: Mean Squared Error of Predictions: Inflation Rate

	Pre-Pandemic	Full Sample
GHS	0.50	3.88
DGHS	0.52	6.34
DHS	0.52	5.18

Note: The table shows the mean squared error (MSE) of the predictions of the inflation rate under the gamma horseshoe (GHS), dynamic gamma horseshoe (DGHS) and dynamic horseshoe (DHS) priors over two prediction samples: the pre-pandemic subsample from Q1 2004 to Q4 2019 and the full sample from Q1 2004 to Q2 2022. A smaller MSE implies more accurate point forecasts on average.

Figure 1: Comparing Shrinkage Parameter

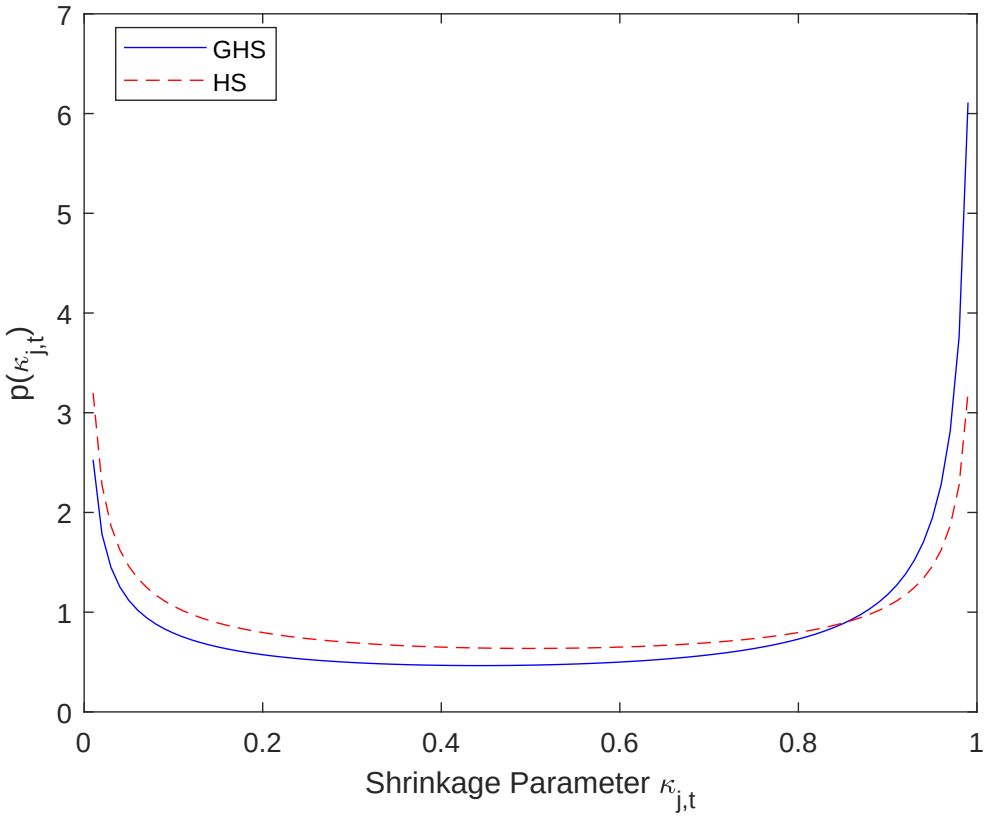

Note: The shrinkage parameter is $\kappa_{j,t} = \frac{1}{1+\phi_{j,t}}$ where $\phi_{j,t}$ is the variance of the differenced time-varying parameter $\Delta\beta_{j,t}$. The details are in Section 2.1.1. The label "HS" refers to the simplified horseshoe prior (dash line) while the label "GHS" refers to the simplified gamma horseshoe prior (solid line).

Figure 2: Regression Coefficient Estimates: Simulation

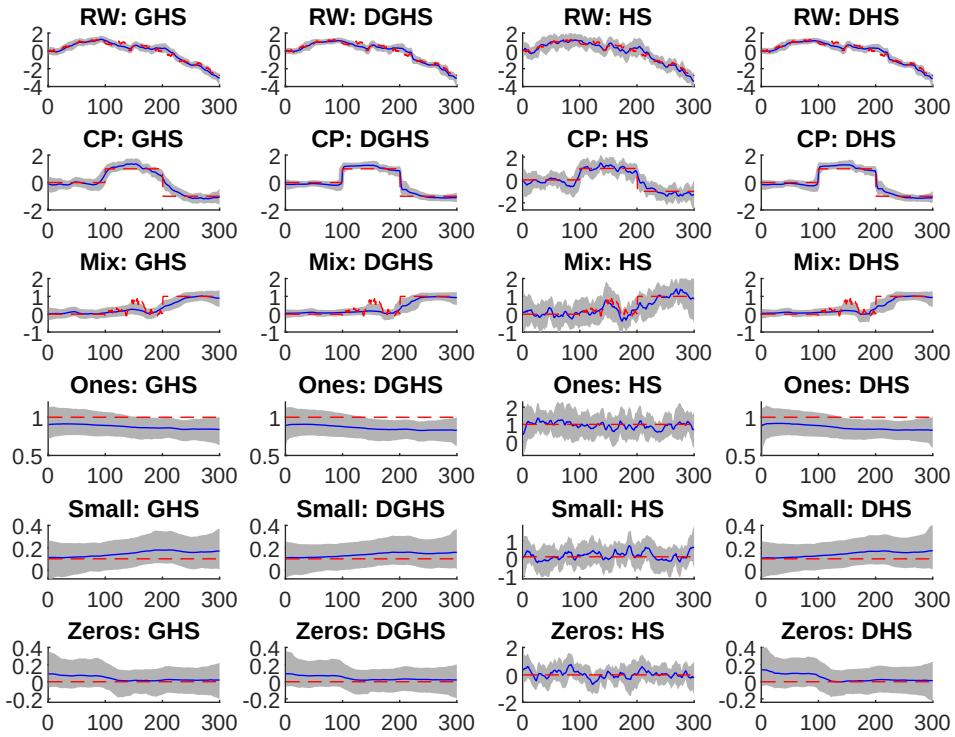

Note: The figure shows the point-wise posterior medians and 90% credible sets of estimated coefficient $\beta_{j,t}$ over time points $t = 1, ..., 300$ for each coefficient $j = 1, ..., 6$ under the 4 TVP priors: gamma horseshoe (GHS), dynamic gamma horseshoe (DGHS), horseshoe (HS) and dynamic horseshoe (DHS). In each subplot, the solid line is the posterior median with the dash line being the true coefficient value and the grey area being the 90% credible set.

Figure 3: Root Mean Squared Error of Coefficient Estimates: Simulation

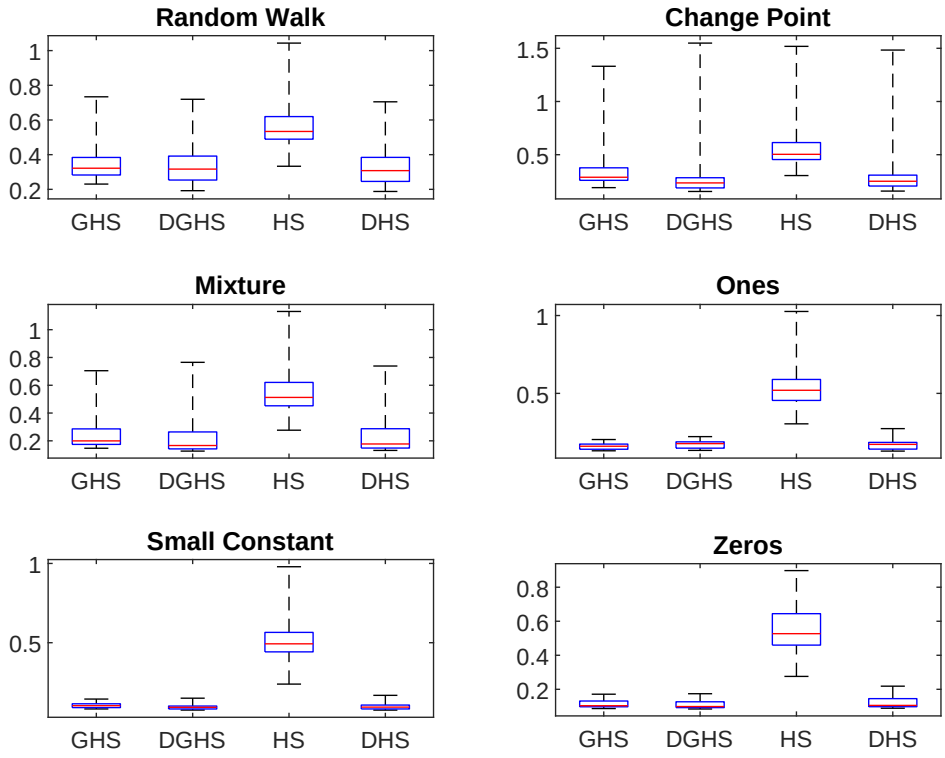

Note: The figure shows the box plots of the root mean squared errors (Equation (11)) of estimated coefficient $\beta_{j,t}$ over time points $t = 1, ..., 300$ for each coefficient $j = 1, ..., 6$ under the 4 TVP priors: gamma horseshoe (GHS), dynamic gamma horseshoe (DGHS), horseshoe (HS) and dynamic horseshoe (DHS). On each box, the central mark indicates the median, and the bottom and top edges of the box indicate the 25^{th} and 75^{th} percentiles respectively. The whiskers extend to the most extreme data points.

Figure 4: Sampling Efficiency Gain by ASIS Boosting: Simulation

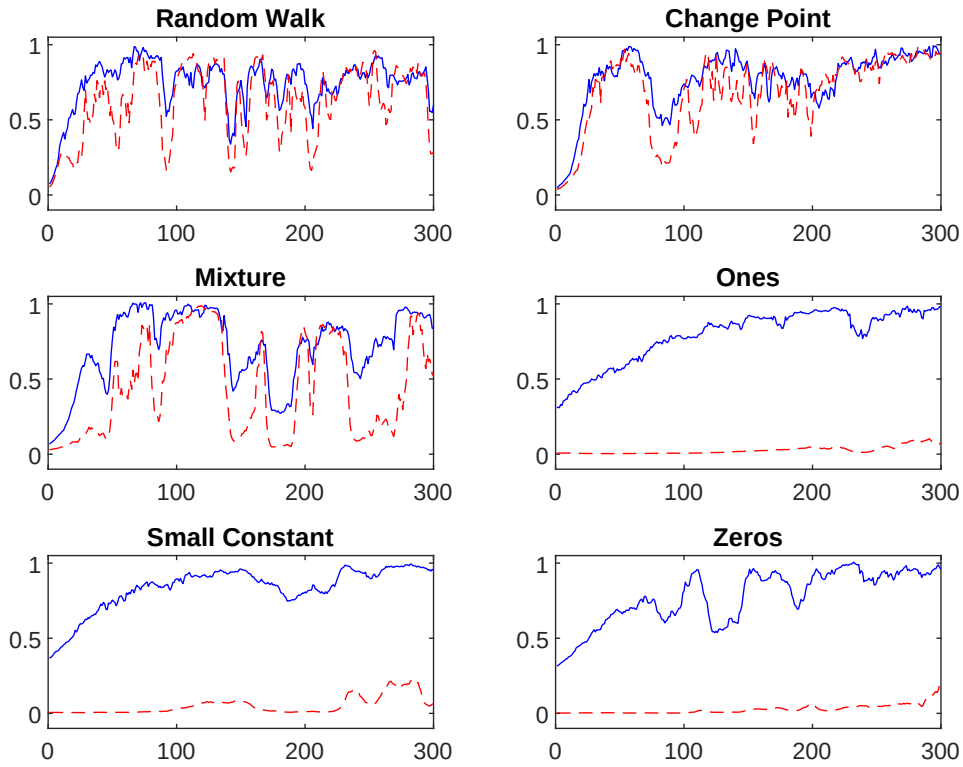

Note: The figure compares the point-wise effective sample size (ESS) of estimated coefficient $\beta_{j,t}$ by a standard Gibbs sampler (dash line) and the ASIS-boosted algorithm (solid line) over time points $t = 1, ..., 300$ for each coefficient $j = 1, ..., 6$ under the gamma horseshoe (GHS) prior. The ESS is normalized by dividing by the number of posterior draws. A higher ESS indicates greater sampling efficiency.

Figure 5: Comparing Sampling Efficiency of Regression Coefficients: Simulation

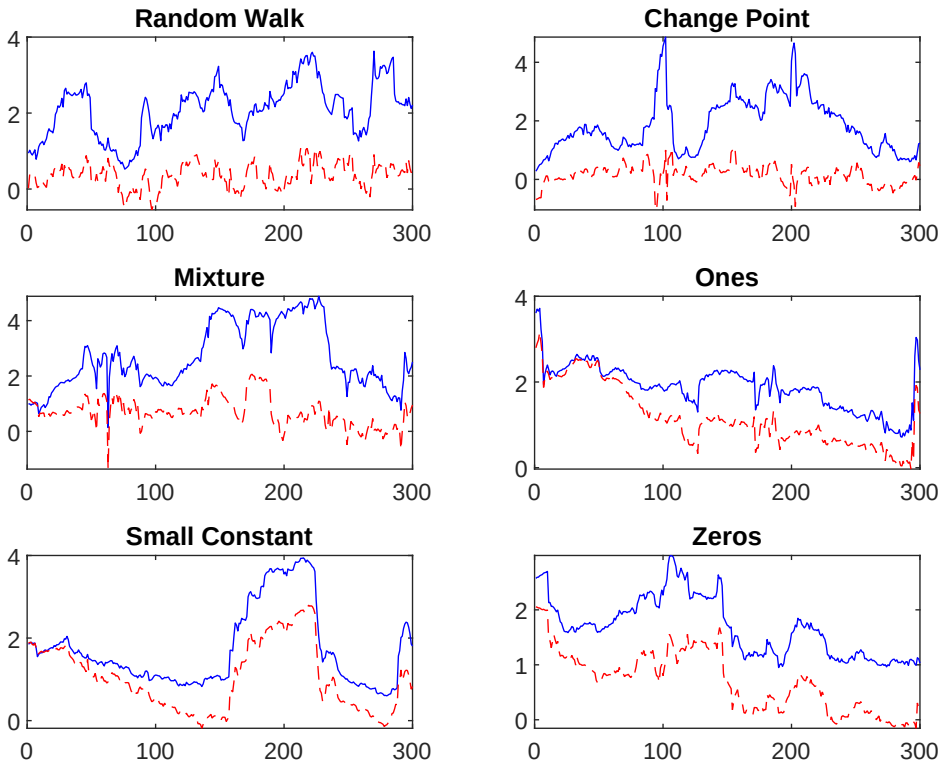

Note: The figure shows the logarithm of the ratio of the point-wise effective sample size (ESS) of estimated coefficient $\beta_{j,t}$ under the gamma horseshoe (GHS, solid line) and dynamic gamma horseshoe (DGHS, dash line) priors to that under the dynamic horseshoe (DHS) prior over time points $t = 1, ..., 300$ for each coefficient $j = 1, ..., 6$. A positive value of the log ESS ratio indicates greater sampling efficiency over the DHS prior.

Figure 6: Data for Empirical Application: Inflation Rate

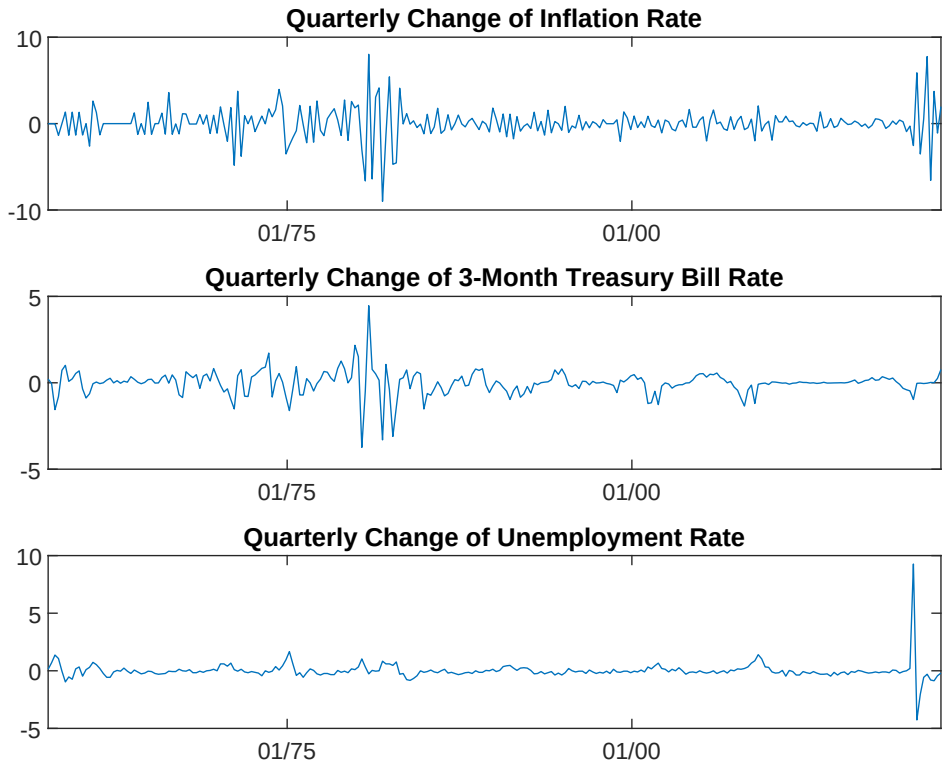

Note: The data source is the FRED database of the U.S. federal reserve bank of St. Louis. The data sample is from Q2 1957 to Q2 2022. The series "inflation rate" is the annualized log quarterly inflation rate based on the U.S. core consumer price index. For the interest rate and unemployment rate, their quarterly values are the average monthly values within each quarter.

Figure 7: Estimates by the Gamma Horseshoe Prior: Inflation Rate

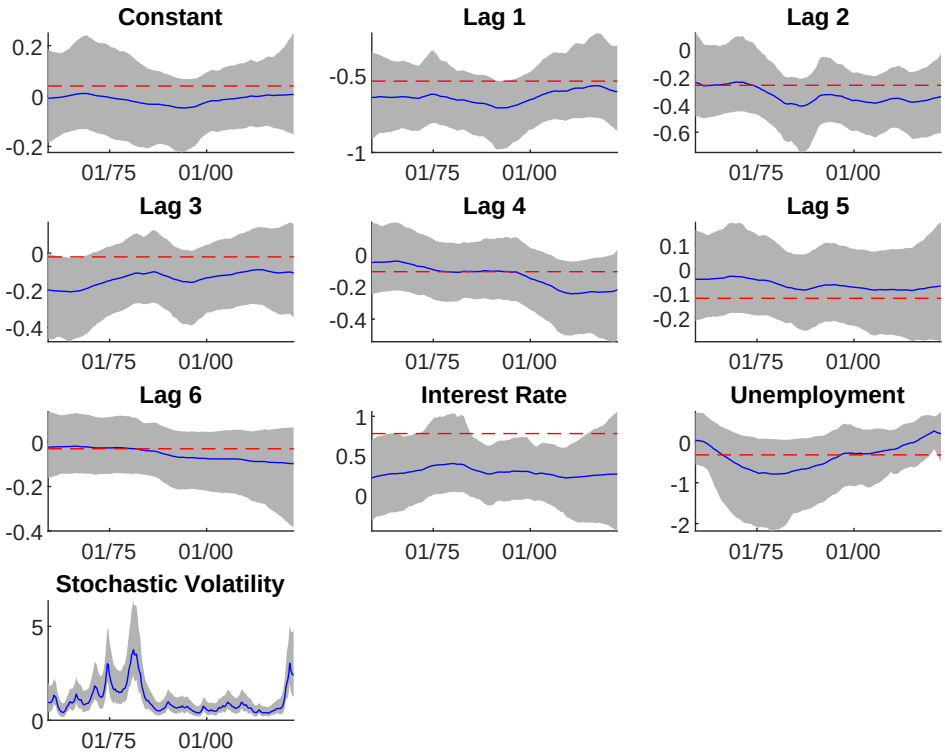

Note: The first 9 panels show the point-wise posterior median (solid line) and 90% credible sets (grey shade) of the coefficients β_t under the gamma horseshoe (GHS) prior where the dash line is the OLS estimate. The last panel shows the point-wise posterior median (solid line) and 90% credible sets (grey shade) of the square root $\sigma_t = \sqrt{\sigma_t^2}$ of the stochastic variance.

Figure 8: Comparing Sampling Efficiency of Regression Coefficients: Inflation

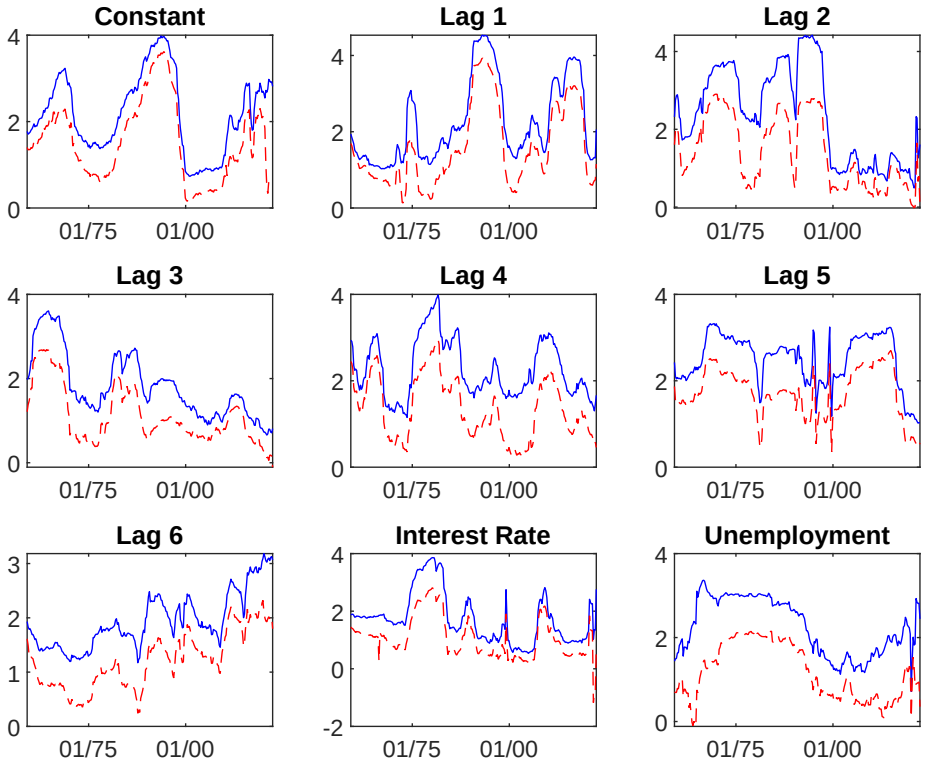

Note: The figure shows the logarithm of the ratio of the point-wise effective sample size (ESS) of estimated coefficient $\beta_{j,t}$ under the gamma horseshoe (GHS, solid line) and dynamic gamma horseshoe (DGHS, dash line) priors to that under the dynamic horseshoe (DHS) prior for each coefficient $j = 1, ..., 9$. A positive value of the log ESS ratio indicates greater sampling efficiency over the DHS prior.

Figure 9: Difference in Cumulative Log Predictive Likelihoods: Inflation Rate

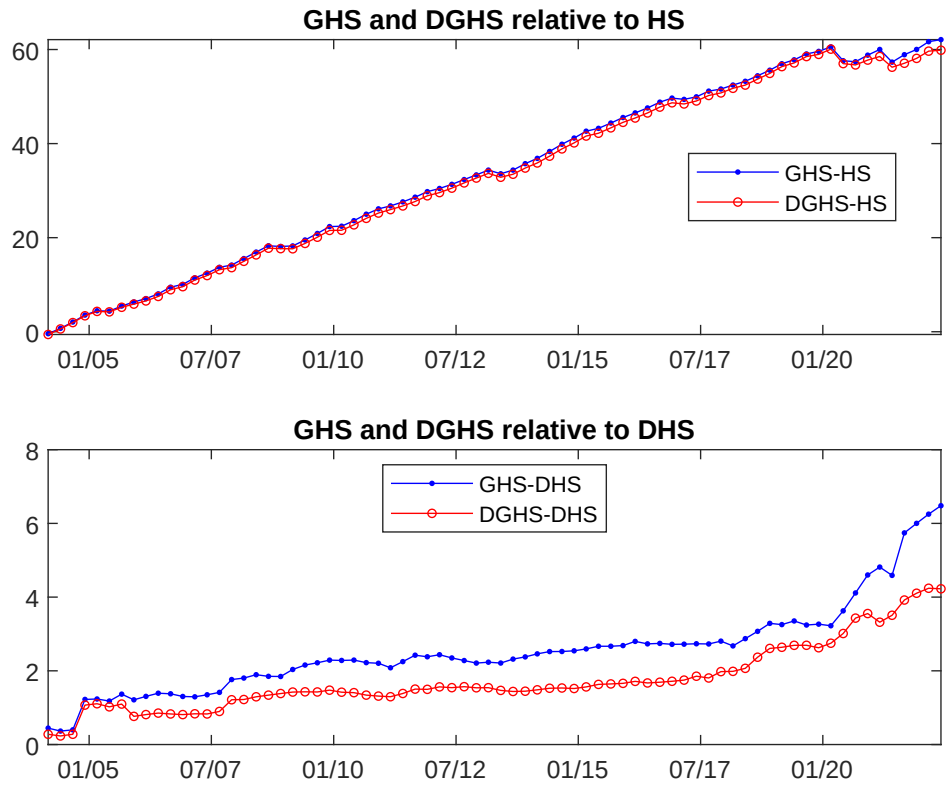

Note: The line with the point marker (·) is the difference in the cumulative log predictive likelihood of the gamma horseshoe (GHS) prior relative to that of the horseshoe (HS) prior (the upper panel) and the dynamic horseshoe (DHS) prior (lower panel). The line with the circle marker (○) is the difference in the cumulative log predictive likelihood of the dynamic gamma horseshoe (DGHS) prior relative to that of the HS prior (the upper panel) and the DHS prior (lower panel).

Appendix

A Conditional Density of Shrinkage Parameter

Following the notations in Section 2.1.1, here I examine the conditional distribution of the shrinkage parameter $\kappa_{j,t}$ under the GHS and HS priors. Based on the representation for a generic variable $\mathcal{X}$ (Makalic and Schmidt (2016)):

$$\mathcal{X} \sim IB(0.5, 0.5) \Longleftrightarrow \mathcal{X}|\lambda \sim IG\left(0.5, \frac{1}{\lambda}\right), \quad \lambda \sim IG(0.5, 1)$$

one can derive the density of $\kappa_{j,t}$ conditional on an auxiliary variable $\lambda_{j,t} \sim IG(0.5, 1)$ under the GHS prior as:

$$p_G(\kappa_{j,t}|\lambda_{j,t}) = \frac{1}{\pi(2\kappa_{j,t} + \lambda_{j,t}(1-\kappa_{j,t}))}\sqrt{\frac{2\lambda_{j,t}}{\kappa_{j,t}(1-\kappa_{j,t})}}$$

Similarly, the conditional density of $\kappa_{j,t}$ under the HS prior can be written as:

$$p_H(\kappa_{j,t}|\lambda_{j,t}) = \frac{1}{\sqrt{\pi\lambda_{j,t}\kappa_{j,t}(1-\kappa_{j,t})^3}} \exp\left(-\frac{\kappa_{j,t}}{\lambda_{j,t}(1-\kappa_{j,t})}\right)$$

Figure A1 compares the logarithm of the conditional densities of $\kappa_{j,t}$ under the HS and GHS priors conditional on $\lambda_{j,t} = 1.2$, 4.4 and 31.2 respectively, which are about the 20^{th}, 50^{th} and 80^{th} percentiles of the distribution $IG(0.5, 1)$. With different values of $\lambda_{j,t}$, the conditional density of $\kappa_{j,t}$ under the GHS prior remains a desirable "U" shape that contains large probability mass around the two ends of $\kappa_{j,t} = 0$ and 1, while the conditional density of $\kappa_{j,t}$ under the HS prior becomes very small towards the end $\kappa_{j,t} = 1$ and hence offers more limited shrinkage. Let $f(\kappa_{j,t}, \lambda_{j,t}) = \frac{p_G(\kappa_{j,t}|\lambda_{j,t})}{p_H(\kappa_{j,t}|\lambda_{j,t})}$. It is useful to note that $\lim_{\kappa_{j,t}\to 0} f(\kappa_{j,t}, \lambda_{j,t}) = \sqrt{\frac{2}{\pi}} \approx 0.8$ while $\lim_{\kappa_{j,t}\to 1} f(\kappa_{j,t}, \lambda_{j,t}) = +\infty$ for a given finite $\lambda_{j,t}$. Therefore the GHS prior allocates more probability mass towards the end of complete shrinkage $\kappa_{j,t} = 1$ than the HS prior while incurring only a limited reduction in the probability mass at the other end of minimal shrinkage $\kappa_{j,t} = 0$. As a result, the GHS prior offers stronger shrinkage than the HS prior but does not over-shrink.

Figure A1: Conditional Density of Shrinkage Parameter

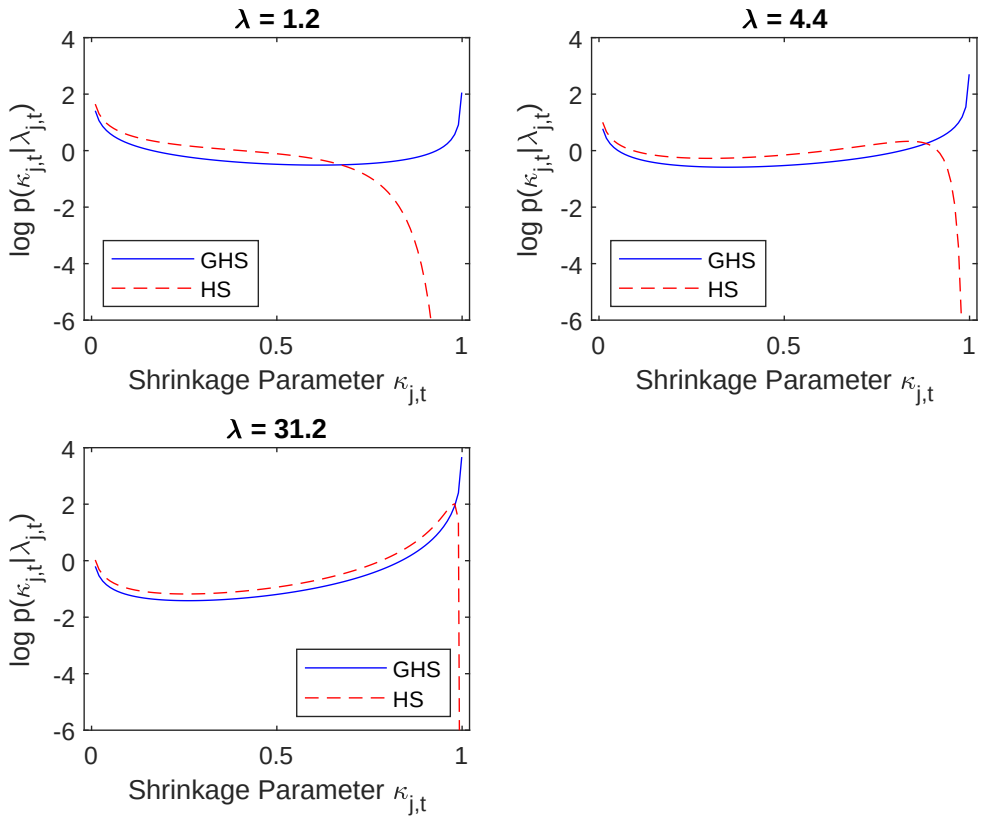

Note: The shrinkage parameter is $\kappa_{j,t} = \frac{1}{1+\phi_{j,t}}$ where $\phi_{j,t}$ is the variance of the differenced time-varying parameter $\Delta\beta_{j,t}$. The parameter $\lambda_{j,t}$ arises from the hierarchical inverse gamma representation of an inverted beta distribution. The details are in Section 2.1.1 and Appendix A. The label "HS" refers to the simplified horseshoe prior (dash line) while the label "GHS" refers to the simplified gamma horseshoe prior (solid line). The y-axis of the log conditional densities are truncated from below for better exposition.

B SV Model Estimation

Estimating the SV model of Equation (2) follows Kastner and Fruhwirth-Schnatter (2014). There are two key ingredients in the method of Kastner and Fruhwirth-Schnatter (2014). The first is the log linearization strategy of Omori et al. (2007) that approximates the logarithm of a $\chi^2(1)$-distributed variable by a mixture of normal distributions and hence transforms a non-linear state space model into a linear one. The second is applying the ASIS strategy of Yu and Meng (2011) that directly boosts the sampling efficiency of the long-run mean and the variance parameter of the volatility process. The details of the method can be found in Kastner and Fruhwirth-Schnatter (2014) and are not repeated here to save space.

The main difference in this paper from Kastner and Fruhwirth-Schnatter (2014) is the prior of the variance parameter in the volatility process. Use the notation of Equation (2). Kastner and Fruhwirth-Schnatter (2014) sets a fixed value for the scale parameter s_y in the gamma prior of the variance parameter $\sigma_y^2 \sim G(0.5, 2s_y)$. This paper instead specifies a prior $s_y \sim IB(0.5, 0.5)$ to determine s_y in a data driven way. The conditional posterior of s_y can be easily derived by applying the hierarchical inverse gamma representation in Makalic and Schmidt (2016): $s_y|a_y, \sigma_y^2 \sim IG\left(1, \frac{1}{a_y} + \frac{\sigma_y^2}{2}\right)$ where a_y is an auxiliary variable with the prior $a_y \sim IG(0.5, 1)$ and the posterior $a_y|s_y \sim IG\left(1, 1 + \frac{1}{s_y}\right)$.

The impact of placing an $IB(0.5, 0.5)$ prior for s_y is studied under the gamma horseshoe prior for time-varying coefficients and by using the inflation rate data of Section 5. The alternative is setting $s_y = 1$ as in the empirical study of Kastner and Fruhwirth-Schnatter (2014). It is found that the posterior median of s_y under the $IB(0.5, 0.5)$ prior is 0.84 with the 90% credible set $(0.04, 19.69)$. So the data is not very informative of s_y and produces a rather dispersed posterior distribution for it. The first panel of Figure B1 compares the posterior of $\sigma_y = \sqrt{\sigma_y^2}$ under $s_y \sim IB(0.5, 0.5)$ and $s_y = 1$. It can be seen that placing an $IB(0.5, 0.5)$ prior for s_y slightly shifts the posterior of σ_y towards zero relative to fixing $s_y = 1$. However, as shown in the two lower panels of Figure B1, the point-wise posterior median and 90% credible set of the square root $\sigma_t = \sqrt{\sigma_t^2}$ of the stochastic variance is very similar across the two approaches of specifying s_y.

Figure B1: Comparing SV Estimates

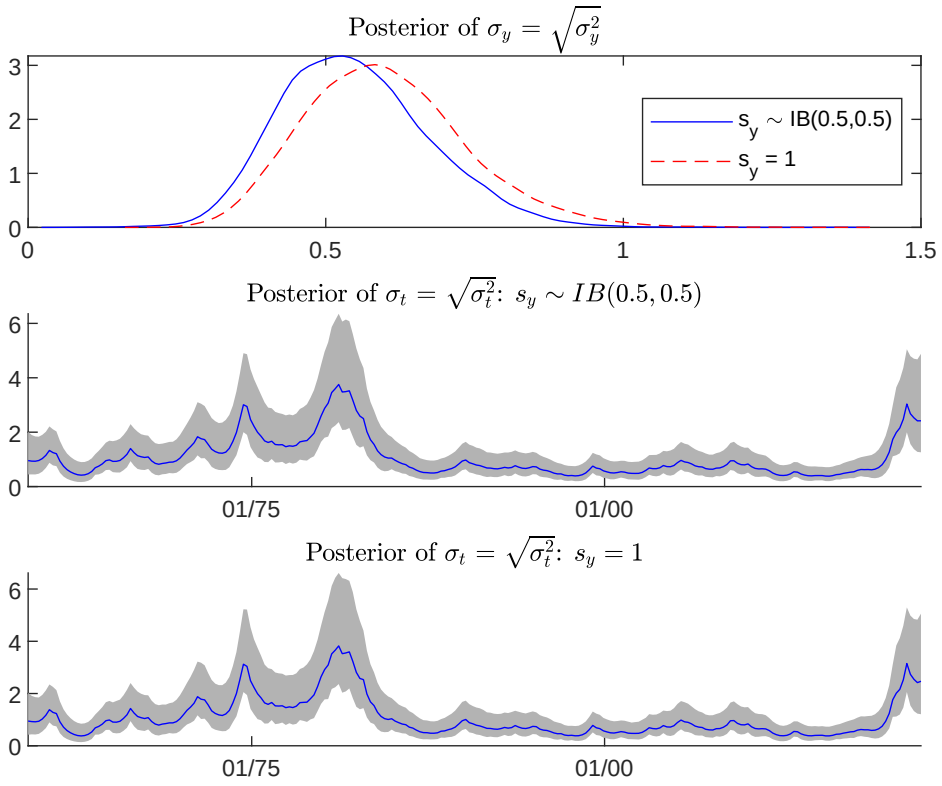

Note: The figure compares the estimate of the stochastic volatility (SV) model under the gamma horseshoe (GHS) prior in the inflation rate data of Section 5 over two scenarios: $s_y \sim IB(0.5, 0.5)$ and $s_y = 1$, where the variance of the SV process $\sigma_y^2 \sim G(0.5, 2s_y)$. The first panel shows the posterior of $\sigma_y = \sqrt{\sigma_y^2}$ under the two specifications of s_y, while the lower two panels show the point-wise posterior median (solid line) and 90% credible set (grey area) of the square root $\sigma_t = \sqrt{\sigma_t^2}$ of the stochastic variance under $s_y \sim IB(0.5, 0.5)$ and $s_y = 1$ respectively.

C Hyper-Parameters of Horseshoe Prior

The horseshoe prior for the square root of the global parameter is $\tilde{v}_j = \pm\sqrt{v_j} \sim N(0, \tau_0\tau_j)$ with $\tau_0 \sim IB(0.5, 0.5)$ and $\tau_j \sim IB(0.5, 0.5)$ for $j = 1, ..., K$. Following Makalic and Schmidt (2016), the inverted beta distributions are represented as hierarchical inverse gamma ones by introducing auxiliary variables:

$$\tau_0 \sim IB(0.5, 0.5) \Longleftrightarrow \tau_0 \sim IG\left(0.5, \frac{1}{a_0}\right), \quad a_0 \sim IG(0.5, 1)$$
$$\tau_j \sim IB(0.5, 0.5) \Longleftrightarrow \tau_j \sim IG\left(0.5, \frac{1}{a_j}\right), \quad a_j \sim IG(0.5, 1)$$

The posteriors can be derived as follows:

$$\tau_0 | a_0, \{\tilde{v}_j\}_{j=1}^K, \{\tau_j\}_{j=1}^K \sim IG\left(\frac{1+K}{2}, \frac{1}{a_0} + \frac{1}{2}\sum_{j=1}^K \frac{1}{\tau_j}\tilde{v}_j^2\right),$$
$$a_0 | \tau_0 \sim IG\left(1, 1 + \frac{1}{\tau_0}\right),$$
$$\tau_j | \tilde{v}_j, \tau_0, a_j \sim IG\left(1, \frac{1}{a_j} + \frac{1}{2\tau_0}\tilde{v}_j^2\right),$$
$$a_j | \tau_j \sim IG\left(1, 1 + \frac{1}{\tau_j}\right).$$

Similarly for the horseshoe prior of the initial state $\beta_{j,0} \sim N(0, \tau_{0,0}\tau_{j,0})$ with $\tau_{0,0} \sim IB(0.5, 0.5)$ and $\tau_{j,0} \sim IB(0.5, 0.5)$ for $j = 1, ..., K$, the hierarchical inverse gamma representation is:

$$\tau_{0,0} \sim IB(0.5, 0.5) \Longleftrightarrow \tau_{0,0} \sim IG\left(0.5, \frac{1}{b_0}\right), \quad b_0 \sim IG(0.5, 1)$$
$$\tau_{j,0} \sim IB(0.5, 0.5) \Longleftrightarrow \tau_{j,0} \sim IG\left(0.5, \frac{1}{b_j}\right), \quad b_j \sim IG(0.5, 1)$$

with the following posteriors:

$$\tau_{0,0} | b_0, \{\beta_{j,0}\}_{j=1}^K, \{\tau_{j,0}\}_{j=1}^K \sim IG\left(\frac{1+K}{2}, \frac{1}{b_0} + \frac{1}{2}\sum_{j=1}^K \frac{1}{\tau_{j,0}}\beta_{j,0}^2\right),$$
$$b_0 | \tau_{0,0} \sim IG\left(1, 1 + \frac{1}{\tau_{0,0}}\right),$$
$$\tau_{j,0} | \beta_{j,0}, \tau_{0,0}, b_j \sim IG\left(1, \frac{1}{b_j} + \frac{1}{2\tau_{0,0}}\beta_{j,0}^2\right),$$
$$b_j | \tau_{j,0} \sim IG\left(1, 1 + \frac{1}{\tau_{j,0}}\right).$$

D Sampling v and β_0 from the SA Representation

Let $\phi = \{\phi_t\}_{t=1}^n$, $\theta_{0,v} = \{\tau_0, \tau_1, ..., \tau_K\}$, $\theta_{0,\beta} = \{\tau_{0,0}, \tau_{0,1}, ..., \tau_{0,K}\}$ and $\mathcal{D} = \{\beta, \phi, \theta_{0,v}, \theta_{0,\beta}\}$. The target is to sample from $p(v, \beta_0|\mathcal{D}) = p(v|\mathcal{D})p(\beta_0|\mathcal{D}, v)$ based on the conditional SA representation of Equation (1).

Given the independent priors $p(v_j|\theta_{0,v}) = G(0.5, 2\tau_0\tau_j)$ for $j = 1, ..., K$, the marginal distribution $p(v|\mathcal{D}) \propto p(v|\theta_{0,v})\ p(\beta|v, \phi, \theta_{0,\beta})$ has no closed form. However one can decompose the likelihood as $p(\beta|v, \phi, \theta_{0,\beta}) = p(\beta_1|v, \phi, \theta_{0,\beta})p(\beta_2, ..., \beta_n|v, \phi, \beta_1)$. The partial posterior $p(v|\theta_{0,v})p(\beta_2, ..., \beta_n|v, \phi, \beta_1)$ would constitute independent generalized inverse Gaussian (GIG) distributions for elements in v. Specifically one can derive:

$$p(v_j|\theta_{0,v}) \prod_{t=2}^{n} p(\beta_{j,t}|v_j, \phi_{j,t}, \beta_{j,t-1}) \propto (v_j)^{-n/2} \exp\left(-\frac{v_j}{2\tau_0\tau_j} - \frac{1}{2v_j}\sum_{t=2}^{n}\frac{(\Delta\beta_{j,t})^2}{\phi_{j,t}}\right) \tag{D1}$$

where $\Delta\beta_{j,t} = \beta_{j,t} - \beta_{j,t-1}$ for $j = 1, ..., K$ and $t = 2, ..., n$. Recognizing that the right-hand side of Equation (D1) is the kernel of the distribution $GIG\left(1 - \frac{n}{2}, \frac{1}{\tau_0\tau_j}, \sum_{t=2}^{n}\frac{(\Delta\beta_{j,t})^2}{\phi_{j,t}}\right)$ for v_j, an independent Metropolis-Hastings step can be readily applied to sample from $p(v_j|\mathcal{D})$ by using the proposal $GIG\left(1 - \frac{n}{2}, \frac{1}{\tau_0\tau_j}, \sum_{t=2}^{n}\frac{(\Delta\beta_{j,t})^2}{\phi_{j,t}}\right)$ for $j = 1, ..., K$[14]. The initial item of the likelihood $p(\beta_1|v, \phi, \theta_{0,\beta}) = \int p(\beta_1|v, \phi, \beta_0)p(\beta_0|\theta_{0,\beta})d\beta_0 = N(0, \text{diag}(v \odot \phi_1 + v_{\beta,0}))$ can be computed by recognizing $p(\beta_1|v, \phi, \beta_0) = N(\beta_0, \text{diag}(v \odot \phi_1))$ and $p(\beta_0|\theta_{0,\beta}) = N(0, \text{diag}(v_{\beta,0}))$, where the j^{th} element of $v_{\beta,0}$ is $\tau_{0,0}\tau_{0,j}$ for $j = 1, ..., K$.

The conditional distribution $p(\beta_0|\mathcal{D}, v) \propto p(\beta_0|\theta_{0,\beta})p(\beta_1|v, \phi, \beta_0)$ is normal thanks to the normal prior $p(\beta_0|\theta_{0,\beta})$ and the normal likelihood $p(\beta_1|v, \phi, \beta_0)$. It is straightforward to derive the posterior $p(\beta_{0,j}|\mathcal{D}, v) = N(b_j, B_j)$ where $B_j = \frac{\tau_{0,0}\tau_{j,0}v_j\phi_{j,1}}{\tau_{0,0}\tau_{j,0}+v_j\phi_{j,1}}$ and $b_j = \frac{\tau_{0,0}\tau_{j,0}\beta_{j,1}}{\tau_{0,0}\tau_{j,0}+v_j\phi_{j,1}}$ for $j = 1, ..., K$.

[14]Sampling from the GIG distribution is by adapting the Matlab function **gigrnd** written by Enes Makalic and Daniel Schimidt that implements an algorithm from Devroye (2014).

E Dynamic Gamma Horseshoe Prior

For convenience, reproduce the SA parametrization of Equation (7) and the equation for $\log(d_{j,t})$:

$$\begin{aligned}
\Delta\beta^*_{j,t} &\sim N(0, \phi_{j,t}) \\
\phi_{j,t} &\sim G(0.5, 2d_{j,t}) \\
\log(d_{j,t}) &= \rho_j \log(d_{j,t-1}) + \log(\xi_{j,t})
\end{aligned}$$

where $\log(d_{j,0}) = 0$, $\log(\xi_{j,t}) \sim N\left(0, \frac{1}{e_{j,t}}\right)$ and $e_{j,t} \sim PG(1,0)$ for $j = 1, ..., K$ and $t = 1, ..., n$. The posterior of the scaled state variance can be derived as:

$$\phi_{j,t}|\beta^*_{j,t}, d_{j,t} \sim GIG\left(0, \frac{1}{d_{j,t}}, \left(\Delta\beta^*_{j,t}\right)^2\right)$$

If one starts the ASIS block from the AA representation (Equation (8)):

$$\begin{aligned}
\Delta\beta^*_{j,t} &\sim N(0, \phi^*_{j,t} d_{j,t}) \\
\phi^*_{j,t} &\sim G(0.5, 2) \\
\log(d_{j,t}) &= \rho_j \log(d_{j,t-1}) + \log(\xi_{j,t})
\end{aligned}$$

The posterior of the transformed latent variable is:

$$\phi^*_{j,t}|\beta^*_{j,t}, d_{j,t} \sim GIG\left(0, 1, \frac{\left(\Delta\beta^*_{j,t}\right)^2}{d_{j,t}}\right)$$

To sample the local parameter $d_{j,t}$ from the SA representation of Equation (7), note that it can be viewed as a stochastic volatility following a SV process with the long-run mean of zero. The strategy of Kastner and Fruhwirth-Schnatter (2014) can be applied here to estimate the SV model. Specifically, applying the log linearization strategy of Omori et al. (2007) approximates a $\log\left(\chi^2(1)\right)$ distribution by a 10-component mixture of normals $\sum_{i=1}^{10} \pi_i N(\mu^*_i, h^*_i)$ and transforms the distribution $\phi_{j,t}|d_{j,t} \sim G(0.5, 2d_{j,t})$[15] into a normal one: $\log(\phi_{j,t})|d_{j,t} \sim N\left(\mu^*_{s_{j,t}} + \log(d_{j,t}), h^*_{s_{j,t}}\right)$ where $s_{j,t} \in \{1, 2, ..., 10\}$ is an indicator for the 10-component-mixture-normal distribution. The posterior for the indicator is:

$$p(s_{j,t} = i|\phi_{j,t}, d_{j,t}) \propto (h^*_i)^{-\frac{1}{2}} \exp\left(-\frac{1}{2h^*_i}\left(\log(\phi_{j,t}) - \mu^*_i - \log(d_{j,t})\right)^2\right)\pi_i$$

[15] A Gamma distribution $G(0.5, 2)$ is equivalent to a $\chi^2(1)$ distribution.

To sample $\log(d_{j,t})$, the precision-based algorithm of Rue (2001) and McCausland et al. (2011) is used. Let $\tilde{d}_j$ be a n-by-1 vector collecting $\log(d_{j,1})$, ..., $\log(d_{j,n})$, $\tilde{y}_j$ be a n-by-1 vector collecting $\log(\phi_{j,1}) - \mu^*_{s_{j,1}}$, ..., $\log(\phi_{j,n}) - \mu^*_{s_{j,n}}$, H be a n-by-n lower bi-diagonal matrix with ones in the diagonal and $-\rho_j$ in each $(i, i-1)$ element for $i = 2$, ..., n, P be a n-by-n diagonal matrix with diagonal elements $h^*_{s_{j,1}}$, ..., $h^*_{s_{j,n}}$ and Q be a n-by-n diagonal matrix with diagonal elements $\frac{1}{e_{j,1}}$, ..., $\frac{1}{e_{j,n}}$. It follows that the posterior for $\tilde{d}_j$ is $N(b_d, B_d)$ where $B_d^{-1} = H'Q^{-1}H + P^{-1}$ and $B_d^{-1}b_d = P^{-1}\tilde{y}_j$. The key for efficient computation is to note that the matrix B_d^{-1} is a tri-diagonal band matrix. Hence a Cholesky decomposition of B_d^{-1} can be efficiently computed by back-substitution and be directly used to draw $\tilde{d}_j$ from the posterior $N(b_d, B_d)$.

Similarly one can sample the local parameter $\log(d_{j,t})$ from the AA representation of Equation (8). Conditional on $\phi^*_{j,t}$, one can write $\frac{\Delta\beta^*_{j,t}}{\sqrt{\phi^*_{j,t}}} \sim N(0, d_{j,t})$. Hence the local parameter $d_{j,t}$ can be recast as the stochastic volatility in a SV process with $\frac{\left(\Delta\beta^*_{j,t}\right)^2}{\phi^*_{j,t}}$ being the observation variable. Sampling of $\log(d_{j,t})$ follows the same steps as in the SA representation by replacing the observation variable $\phi_{j,t}$ with the new one $\frac{\left(\Delta\beta^*_{j,t}\right)^2}{\phi^*_{j,t}}$.

Conditional on $d_{j,t}$, its hyper-parameters ρ_j and $e_{j,t}$ can be sampled as follows. Given the prior $\rho_j \sim N(\mu_\rho, h_\rho) I_{\{-1<\rho_j<1\}}$, a Metropolis-Hasting step is used to sample ρ_j by a proposal $N(a_\rho, b_\rho)$ where $b_\rho^{-1} = h_\rho^{-1} + \sum_{t=1}^n e_{j,t} \left(\log(d_{j,t-1})\right)^2$ and $b_\rho^{-1}a_\rho = h_\rho^{-1}\mu_\rho + \sum_{t=1}^n e_{j,t}\log(d_{j,t-1})\log(d_{j,t})$. This paper sets $\mu_\rho = 0.95$ to reflect the prior belief that $d_{j,t}$, being the stochastic volatility of a SV process, is highly persistent and at the same time sets $h_\rho = 1$ to allow a large degree of uncertainty for this prior belief.

Following Kowal et al. (2019), the posterior for $e_{j,t}$ is $e_{j,t}|d_{j,t}, \rho_j \sim PG(1, \log(d_{j,t}) - \rho_j\log(d_{j,t-1}))$[16]. This completes the sampling steps for the dynamic gamma horseshoe prior.

[16]Sampling from the polya-gamma distribution is by the Matlab function **pgdraw** written by Enes Makalic and Daniel Schimidt that implements an algorithm from Windle (2013).

F Kalman Filter

The iterations to derive the conditional filtering distribution $p(\beta_n|y^n, x^n, \theta^n)$ are adapted from Bitto and Fruhwirth-Schnatter (2019) and are provided below using the notation of Equation (1):

- Start with the initial state $\beta_0 \sim N(b_0, B_0)$ where $b_0 = 0$ and $B_0 = \text{diag}(\tau_0\tau_1, ..., \tau_0\tau_K)$.
- Iterate forward over a prediction step and a filtering step for $t = 1, ..., n$:
  - $\beta_t|\mathcal{I}_{t-1} \sim N(b_{t-1}, R_t)$ with $R_t = B_{t-1} + \text{diag}(w_t)$;
  - $\beta_t|\mathcal{I}_t \sim N(b_t, B_t)$ with $b_t = b_{t-1} + K_t(y_t - \hat{y}_t)$ and $B_t = (I_K - K_t x_t')R_t$, where $\hat{y}_t = x_t' b_{t-1}$, $K_t = R_t x_t S_t^{-1}$ and $S_t = x_t' R_t x_t + \sigma_t^2$.

where $\mathcal{I}_t$ denotes the information set $\{y^t, x^t, \theta^n\}$ at time t.

G Additional Results of Empirical Study

Figure G1 and G2 show the point-wise posterior median and 90% credible set of β_t by the 4 TVP prior specifications: GHS, DGHS, HS and DHS, while Figure G3 compares the square root $\sigma_t = \sqrt{\sigma_t^2}$ of the stochastic variance. The estimated β_t by the GHS, DGHS and DHS priors are generally similar, though the 90% credible set of β_t by the GHS prior tends to be somewhat narrower than the DGHS and DHS priors. The estimated σ_t by the GHS, DGHS and DHS priors are very close and are hardly distinguishable by examining their point-wise posterior median and 90% credible set. Of note, the spikes of inflation rates in the late 1970s and the COVID pandemic are captured by the estimated σ_t rather than the time-varying coefficients β_t in the estimates of these 3 TVP priors.

Estimates by the HS prior are different from the other TVP priors. The point-wise posterior median of β_t by the HS prior is directionally consistent with the other TVP priors but is markedly more volatile. Moreover, the point-wise 90% credible set of β_t by the HS prior is significantly wider than the other TVP priors. Comparing the estimated σ_t (Figure G3) reveals that the HS prior produces smaller and smoother estimate of σ_t than the other TVP priors and hence attributes many fluctuations in the inflation rate to the time-varying coefficients β_t rather than to the stochastic variance σ_t^2.

Figure G1: Estimated Coefficients β_t for Inflation Rate: Part I

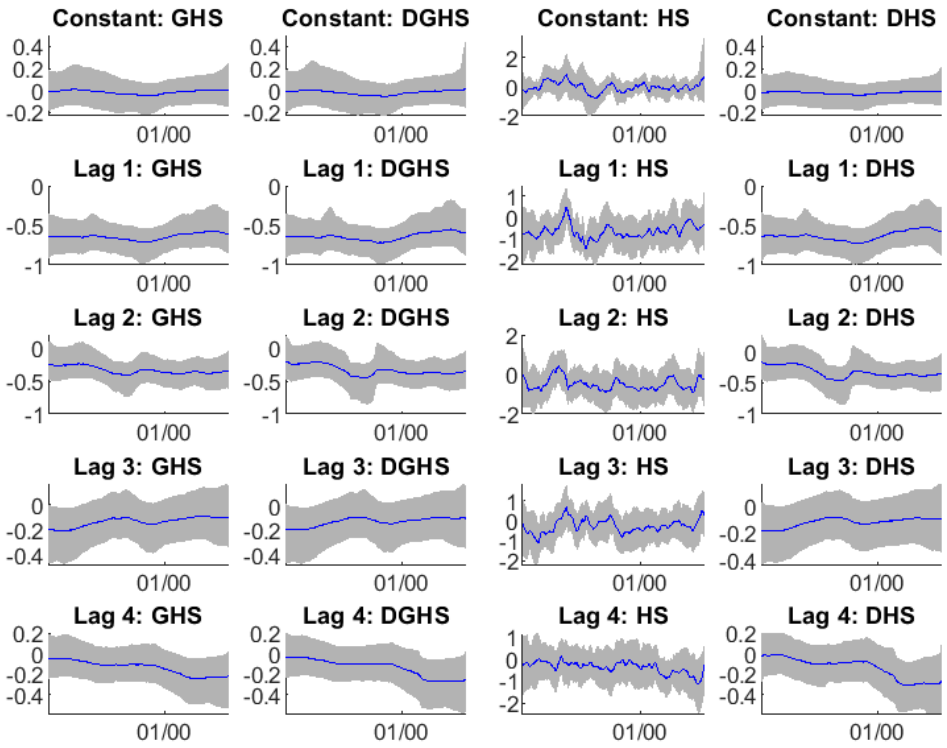

Note: The figure shows the point-wise posterior median (solid line) and 90% credible set (grey area) of the coefficients β_t for the inflation rate study of Section 5 under the gamma horseshoe (GHS), dynamic gamma horseshoe (DGHS), horseshoe (HS) and dynamic horseshoe (DHS) priors. For ease of exposition, this figures shows the coefficients for the constant and autoregressive lags 1 to 4.

Figure G2: Estimated Coefficients β_t for Inflation Rate: Part II

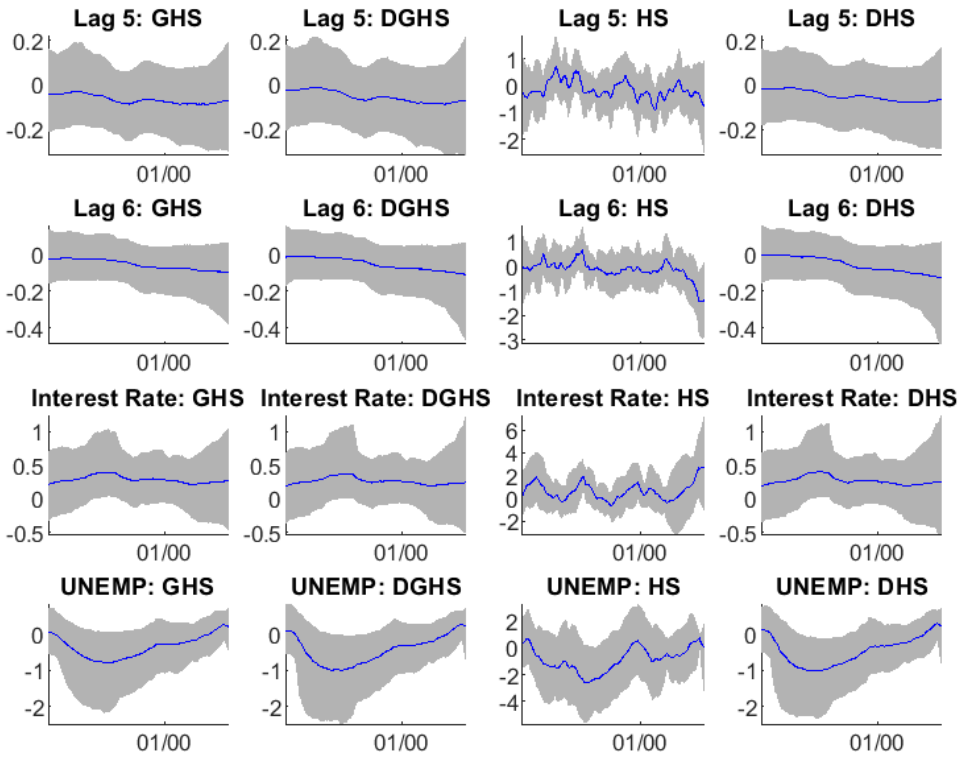

Note: The figure shows the point-wise posterior median (solid line) and 90% credible set (grey area) of the coefficients β_t for the inflation rate study of Section 5 under the gamma horseshoe (GHS), dynamic gamma horseshoe (DGHS), horseshoe (HS) and dynamic horseshoe (DHS) priors. For ease of exposition, this figures shows the coefficients for autoregressive lags 5 to 6, interest rate and unemployment rate (UNEMP).

Figure G3: Estimated SV for Inflation Rate

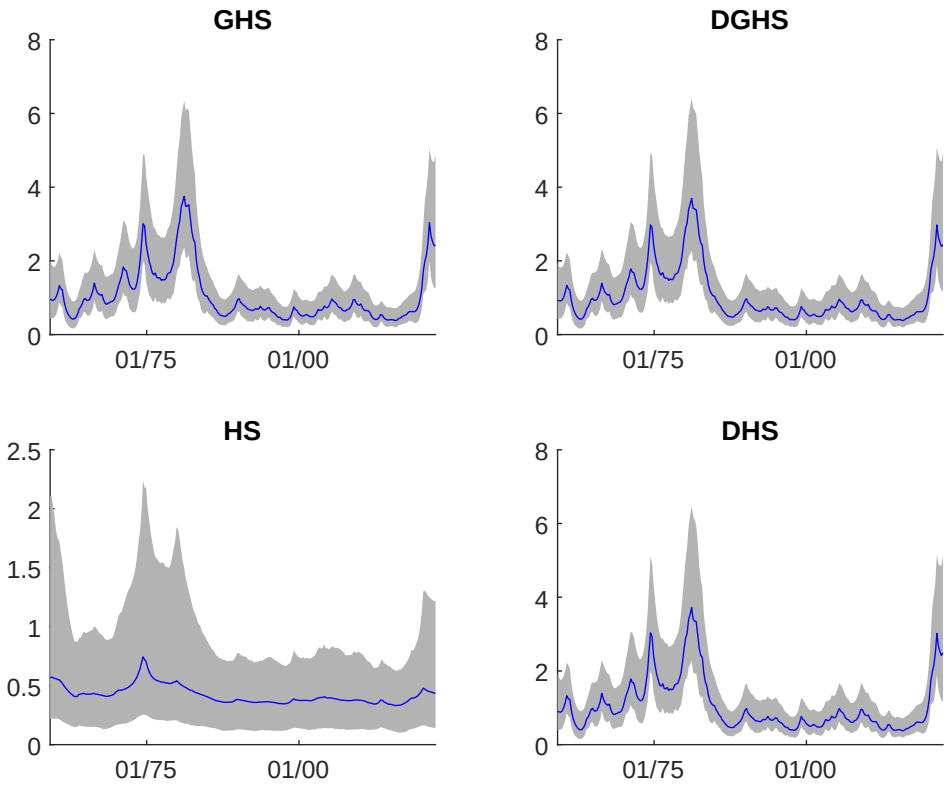

Note: The figure shows the point-wise posterior median (solid line) and 90% credible set (grey area) of the square root $\sigma_t = \sqrt{\sigma_t^2}$ of the stochastic variance for the inflation rate study of Section 5 under the gamma horseshoe (GHS), dynamic gamma horseshoe (DGHS), horseshoe (HS) and dynamic horseshoe (DHS) priors.

References

Abramowitz, M. and I. Stegun (Eds.) (1973). *Handbook of Mathematical Functions*. New York: Dover Publications.

Barndorff-Nielsen, O., J. Kent, and M. Sorensen (1982). Normal variance-mean mixtures and z distributions. *International Statistical Review 50*, 145–159.

Belmonte, M., G. Koop, and D. Korobolis (2014). Hierarchical shrinkage in time-varying parameter models. *Journal of Forecasting 33*, 80–94.

Bhadra, A., J. Datta, N. Polson, and B. Willard (2019). Lasso meets horseshoe: A survey. *Statistical Science 34* (3), 405–427.

Bhattacharya, A., A. Chakraborty, and B. Mallick (2016). Fast sampling with gaussian scale mixture priors in high-dimensional regression. *Biometrika 103* (4), 985–991.

Bitto, A. and S. Fruhwirth-Schnatter (2019). Achieving shrinkage in a time-varying parameter model framework. *Journal of Econometrics 210*, 75–97.

Cadonna, A., S. Fruhwirth-Schnatter, and P. Knaus (2020). Triple the gamma - a unifying shrinkage prior for variance and variable selection in sparse state space and tvp models. *Econometrics 8* (2), 20.

Carriero, A., T. Clark, and M. Marcellino (2019). Large bayesian vector autoregressions with stochastic volatility and non-conjugate priors. *Journal of Econometrics 212* (1), 137–154.

Carvalho, C., N. Polson, and J. Scott (2010). The horseshoe estimator for sparse signals. *Biometrika 97*, 465–480.

Chan, J., E. Eisenstat, and R. Strachan (2020). Reducing the state space dimension in a large tvp-var. *Journal of Econometrics 218*, 105–118.

Chan, J., G. Koop, R. Leon-Gonzalez, and R. Strachan (2012). Time varying dimension models. *Journal of Business and Economic Statistics 30* (3), 358–367.

Chib, S. (1998). Estimation and comparison of multiple change-point models. *Journal of Econometrics 86*(2), 221–241.

Cogley, T. and T. Sargent (2005). Drifts and volatilities: Monetary policies and outcomes in the post wwii u.s. *Review of Economic Dynamics 8*, 262–302.

Dangl, T. and M. Halling (2012). Predictive regressions with time-varying coefficients. *Journal of Financial Economics 106*, 157–181.

Devroye, L. (2014). Random variate generation for the generalized inverse gaussian distribution. *Statistics and Computing 24*, 239–246.

Diebold, F. and R. Mariano (1995). Comparing predictive accuracy. *Journal of Business and Economic Statistics 13*, 253–263.

Dufays, A. and J. Rombouts (2020). Relevant parameter changes in structural break models. *Journal of Econometrics 217*, 46–78.

Durbin, J. and S. Koopman (2002). A simple and efficient simulation smoother for state space time series analysis. *Biometrika 89*, 603–615.

Fruhwirth-Schnatter, S. (1994). Data augmentation and dynamic linear models. *Journal of Time Series Analysis 15*, 183–202.

Fruhwirth-Schnatter, S. (2004). Efficient bayesian parameter estimation. In A. Harvey, S. Koopman, and N. Shephard (Eds.), *State Space and Unobserved Component Models: Theory and Applications*, pp. 123–151. Cambridge University Press.

Fruhwirth-Schnatter, S. and H. Wagner (2010). Stochastic model specification search for gaussian and partially non-gaussian state space models. *Journal of Econometrics 154*, 85–100.

George, E. and R. McCulloch (1993). Variable selection via gibbs sampling. *Journal of the American Statistical Association 88*, 881–889.

Geweke, J. and G. Amisano (2010). Comparing and evaluating bayesian predictive distributions of asset returns. *International Journal of Forecasting 26*, 216–230.

Geyer, C. (1992). Practical markov chain monte carlo. *Statistical Science 7*, 473–483.

Giordani, P. and R. Kohn (2008). Efficient bayesian inference for multiple change-point and mixture innovation models. *Journal of Business and Economic Statistics 26*, 66–77.

Granger, C. (2008). Non-linear models: Where do we go next - time varying parameter models? *Studies in Nonlinear Dynamics & Econometrics 12*, 1–11.

Griffin, J. and P. Brown (2010). Inference with normal-gamma prior distributions in regression problems. *Bayesian Analysis 5*(1), 171–188.

Harvey, C. (1989). Forecasts of economic growth from the bond and stock markets. *Financial Analysts Journal 45*(5), 38–45.

Hauzenberger, N. (2021). Flexible mixture priors for large time-varying parameter models. *Econometrics and Statistics 20*, 87–108.

Hauzenberger, N., F. Huber, and G. Koop (2020). Dynamic shrinkage priors for large time-varying parameter regressions using scalable markov chain monte carlo methods. arXiv:2005.03906v1 [econ.EM].

Huber, F. and M. Pfarrhofer (2021). Dynamic shrinkage in time-varying parameter stochastic volatility in mean models. *Journal of Applied Econometrics 36*, 262–270.

Ishwaran, H. and J. Rao (2005). Spike and slab variable selection: frequentist and bayesian strategies. *Annals of Statistics 33*, 730–773.

Johndrow, J., P. Orenstein, and A. Bhattacharya (2020). Scalable approximate mcmc algorithms for the horseshoe prior. *Journal of Machine Learning Research 21*(73), 1–61.

Kalli, M. and J. Griffin (2014). Time-varying sparsity in dynamic regression models. *Journal of Econometrics 178*, 779–793.

Kastner, G. and S. Fruhwirth-Schnatter (2014). Ancillarity-sufficiency interweaving strategy (asis) for boosting mcmc estimation of stochastic volatility models. *Computational Statistics and Data Analysis 76*, 408–423.

Kim, S., N. Shephard, and S. Chib (1998). Stochastic volatility: Likelihood inference and comparison with arch models. *Review of Economic Studies 65*, 361–393.

Kowal, D., D. Matteson, and D. Ruppert (2019). Dynamic shrinkage processes. *Journal of the Royal Statistical Society: Series B (Statistical Methodology) 81*, 781–804.

Lopes, H., R. McCulloch, and R. Tsay (2018). Parsimony inducing priors for large scale state space models. Technical report, Booth School of Business, University of Chicago.

Makalic, E. and D. Schmidt (2016). A simple sampler for the horseshoe estimator. *IEEE Signal Processing Letters 23*(1), 179–182.

McCausland, W., S. Miller, and D. Pelletier (2011). Simulation smoothing for state-space models: A computational efficiency analysis. *Computational Statistics and Data Analysis 55*(1), 199–212.

Nakajima, J. and M. West (2013). Bayesian analysis of latent threshold dynamic models. *Journal of Business and Economic Statistics 31*, 151–164.

Omori, Y., S. Chib, N. Shephard, and J. Nakajima (2007). Stochastic volatility with leverage: Fast and efficient likelihood inference. *Journal of Econometrics 140*, 425–449.

Polson, N. and J. Scott (2012). On the half-cauchy prior for a global scale parameter. *Bayesian Analysis 7*(4), 887–902.

Polson, N., J. Scott, and J. Windle (2013). Bayesian inference for logistic models using polya-gamma latent variables. *Journal of the American Statistical Association 108*(504), 1339–1349.

Primiceri, G. (2005). Time varying structural autoregressions and monetary policy. *Review of Economic Studies 72*(3), 821–852.

Rockova, V. and K. McAlinn (2021). Dynamic variable selection with spike-and-slab process priors. *Bayesian Analysis 16*(1), 233–269.

Rue, H. (2001). Fast sampling of gaussian markov random fields. *Journal of the Royal Statistical Society: Series B (Statistical Methodology) 63*, 325–338.

Simpson, M., J. Niemi, and V. Roy (2017). Interweaving markov chain monte carlo strategies for efficient estimation of dynamic linear models. *Journal of Computational and Graphical Statistics 26*(1), 152–159.

Windle, J. (2013). Forecasting high-dimensional, time-varying variance-covariance matrices with high-frequency data and sampling polya-gamma random variates for posterior distributions derived from logistic likelihoods. University of Texas at Austin, PhD Thesis.

Yu, Y. and X. Meng (2011). To center or not to center: That is not the question - an ancillarity-sufficiency interweaving strategy (asis) for boosting mcmc efficiency. *Journal of Computational and Graphical Statistics 20*(3), 531–570.